J|A|C|S
ARTICLES
Published on Web 09/22/2004

Building Blocks for n-Type Molecular and Polymeric Electronics. Perfluoroalkyl- versus Alkyl-Functionalized Oligothiophenes (nT; $n = 2-6$). Systematics of Thin Film Microstructure, Semiconductor Performance, and Modeling of Majority Charge Injection in Field-Effect Transistors

Antonio Facchetti, Melissa Mushrush, Myung-Han Yoon, Geoffrey R. Hutchison, Mark A. Ratner,* and Tobin J. Marks*

Contribution from the Department of Chemistry and the Materials Research Center, Northwestern University, 2145 Sheridan Road, Evanston, Illinois 60208-3113

Received February 23, 2004; E-mail: ratner@northwestern.edu; t-marks@northwestern.edu

Abstract: The solid-state properties and FET electrical behavior of several series of α,ω- and β,β'-fluorocarbon- and alkyl-substituted and unsubstituted oligothiophenes nTs ($n = 2-6$) are compared and contrasted. The thin films were grown by slow vacuum deposition over a range of substrate temperatures and/or by casting from solution and were investigated by X-ray diffraction and scanning electron microscopy. Our results indicate that vacuum deposition at 60−80 °C affords films with remarkably similar microstructures despite the extensive H → F substitution. Trends in observed *d* spacing versus molecular core extension provide quantitative information on molecular orientation. Field-effect transistor measurements performed for all systems and having the same device structure, components, and fabrication conditions demonstrate that all nTs functionalized with fluorocarbon chains at the thiophene termini are n-type semiconductors, in contrast to the p-type activity of the remaining systems. One of these systems, α,ω-diperfluorohexyl-4T, exhibits a mobility of 0.22 $cm^2/(V\ s)$ and an $I_{on}:I_{off}$ ratio of 10^6, one of the highest so far reported for an n-type organic semiconductor. The effect of substitution regiochemistry on FET majority charge carrier was additionally studied, in the case of a 6T core, by shifting the fluorocarbon substituents from the terminal to the central thiophene units. Finally, we propose a simple theoretical model for electrode/organic interfacial carrier injection. The results suggest why modest substituent-induced changes in the injection barrier can produce working n-type materials.

Introduction

The crucial building block for (micro)electronics is the field-effect transistor (FET), based on inorganic electrodes, insulators, and semiconductors.[1] These devices have proven to be reliable, highly efficient, and with performance that increases regularly according to Moore's law.[2] Instead of competing with conventional silicon technologies, organic FETs based on molecular and polymeric materials (OFETs) may find niche applications in low-performance memory elements and sensors,[3] as well as in integrated optoelectronic devices, such as pixel drive and switching elements in active-matrix organic light-emitting diode (OLED) displays.[4] Such organic systems have been intensively investigated because they offer numerous straightforward attractions: vapor phase or solution fabrication and good compatibility with a variety of substrates, including flexible plastics,[5] and broad opportunities for rational structural tailoring.[6] This trend is driven by the demand for low-cost, large-area, flexible,

(1) Sze, S. M. *Semiconductor Devices: Physics and Technology*; Wiley: New York, 1985; pp 6−7, 216−218, 507−510.
(2) Moore, G. E. *IEEE IEDM Technol. Dig.* **1975**, 11−13.
(3) (a) Mushrush, M.; Facchetti, A.; Lefenfeld, M.; Katz, H. E.; Marks, T. J. *J. Am. Chem. Soc.* **2003**, *125*, 9414. (b) Klauk, H.; Halik, M.; Zschieschang, U.; Eder, F.; Schmid, G.; Dehm, C. *Appl. Phys. Lett.* **2003**, *82*, 4175. (c) Katz, H. E.; Hong, X. M.; Dodabalapur, A.; Sarpeshkar, R. *J. Appl. Phys.* **2002**, *91*, 1572. (d) Singhal, R.; Takashima, W.; Kaneto, K.; Samanta, S. B.; Annapoorni, S.; Malhotra, B. D. *Sens. Actuators, B* **2002**, *86*, 42. (e) Roncali, J. *J. Mater. Chem.* **1999**, *9*, 1875. (f) Velu, G.; Legrand, C.; Tharaud, O.; Chapoton, A.; Remiens, D.; Horowitz, G. *Appl. Phys. Lett.* **2001**, *79*, 659. (g) Bao, Z.; Feng, Y.; Dodabalapur, A.; Raju, V. R.; Lovinger, A. J. *Chem. Mater.* **1997**, *9*, 1299. (h) Drury, C. J.; Mutsaers, C. M. J.; Hart, C. M.; Matters, M.; de Leeuw, D. M. *Appl. Phys. Lett.* **1998**, *73*, 108.
(4) (a) Kitamura, M.; Imada, T.; Arakawa, Y. *Jpn. J. Appl. Phys.* **2003**, *42*, 2483. (b) Huitema, H. E. A.; Gelinck, G. H.; van der Putten, J. B. P. H.; Kuijk, K. E.; Hart, K. M.; Cantatore, E.; de Leeuw, D. M. *Adv. Mater.* **2002**, *14*, 1201. (c) Sheraw, C. D.; Zhou, L.; Huang, J. R.; Gundlach, D. J.; Jackson, T. N.; Kane, M. G.; Hill, I. G.; Hammond, M. S.; Campi, J.; Greening, B. K.; Francl, J.; West, J. *Appl. Phys. Lett.* **2002**, *80*, 1088. (d) Mach, P.; Rodriguez, S. J.; Nortrup, R.; Wiltzius, P.; Rogers, J. A. *Appl. Phys. Lett.* **2001**, *78*, 3592. (e) Sirringhaus, H.; Tessler, N.; Friend, R. H. *Science* **1998**, *280*, 1741. (f) Dodabalapur, A.; Bao, Z.; Makhija, A.; Laquindanum, J. G.; Raju, V. R.; Feng, Y.; Katz, H. E.; Rogers, J. *Appl. Phys. Lett.* **1998**, *73*, 142. (g) Jackson, T. N.; et al. *IEEE J. Sel. Top. Quantum Electron. 4* **1998**, 100.
(5) (a) Wang, Z.; Yuan, J.; Zhang, J.; Xing, R.; Yan, D.; Han, Y. *Adv. Mater.* **2003**, *15*, 1009. (b) Lee, J. H.; Kim, S. H.; Kim, G. H.; Lim, S. C.; Lee, H.; Jang, J.; Zyung, T. *Synth. Met.* **2003**, *139*, 445. (c) Noh, Y.-Y.; Kim, J.-J.; Yase, K.; Nagamatsu, S. *Appl. Phys. Lett.* **2003**, *83*, 1243. (d) Locklin, J.; Shinbo, K.; Onishi, K.; Kaneko, F.; Bao, Z.; Advincula, R. C. *Chem. Mater.* **2003**, *15*, 1404. (e) Halik, M.; Klauk, H.; Zschieschang, U.; Schmid, G.; Radlik, W.; Weber, W. *Adv. Mater.* **2002**, *14*, 1717. (f) Kagan, C. R.; Breen, T. L.; Kosbar, L. L. *Appl. Phys. Lett.* **2001**, *79*, 3536. (g) Sirringhaus, H.; Kawase, T.; Friend, R. H.; Shimoda, T.; Inbasekaran, M.; Wu, W.; Woo, E. P. *Science* **2000**, *290*, 2123. (h) Rogers, J. A.; Bao, Z.; Makhija, A.; Braun, P. *Adv. Mater.* **1999**, *11*, 741. (i) Bao, Z.; Rogers, J. A.; Katz, H. E. *J. Mater. Chem.* **1999**, *9*, 1895.

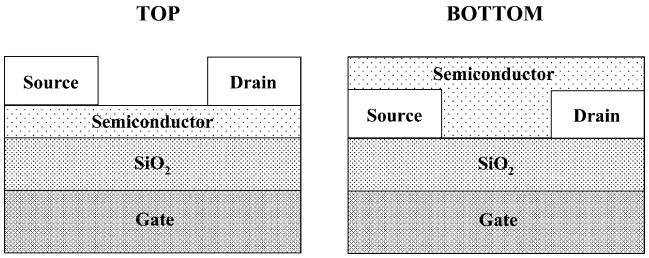

Figure 1. Schematic representation of top- and bottom-configuration TFT devices.

and lightweight devices and the possibility of processing these materials at far lower substrate temperatures as compared to typical inorganic semiconductors.[5]

The simplest and most common OFET device configuration is that of a thin-film transistor (TFT), in which a thin film of the organic semiconductor is deposited on top of a dielectric with an underlying gate (G) electrode (Figure 1). Charge-injecting drain−source (D−S) electrodes providing the contacts are defined either on top of the organic film (top-configuration) or on the surface of the FET substrate prior to deposition of the semiconductor film (bottom-configuration). The current between S and D electrodes is minimal when no voltage is applied between G and D electrodes, and the device is in the so-called "off" state. When a voltage is applied to the gate, charges can be induced into the semiconductor at the interface with the dielectric layer. As a result, the D−S current increases due to the increased number of charge carriers, and this is called the "on" state of the transistor. The key parameters characterizing a FET include the field-effect mobility (μ) which quantifies the average charge carrier drift velocity per unit electric field and the on/off ratio (I_{on}:I_{off}) defined as the D−S current ratio between the "on" and "off" states. For a high-performance OFET, μ and I_{on}:I_{off} should both be as high as possible.

To date, the vast majority of organic FETs operate in the p-type accumulation mode, meaning that the semiconductor acts as a hole-transporting material.[6,7] For full realization of the potential of organic electronics, high-performance electron-transporting (n-type) materials are also needed.[8] For most practical applications, the mobility of the field-induced charges must be $>0.1-1$ cm^2/(V s). To achieve acceptable performance, organic semiconductors must satisfy stringent criteria relating both the injection and the current-carrying characteristics, in particular: (i) the HOMO/LUMO energies of the individual molecules (perturbed by their placement in a crystalline solid) must be at levels where holes/electrons can be incorporated at accessible applied voltages, (ii) the crystal structure of the material must provide sufficient overlap of frontier orbitals to allow efficient charge migration between neighboring molecules, (iii) the solid should be extremely pure because impurities act as charge carrier traps, (iv) the molecules should be preferentially oriented with the long axes approximately parallel to the FET substrate normal because the most efficient charge transport occurs along the direction of intermolecular $\pi-\pi$ stacking, and (v) the crystalline domains of the semiconductor must cover the area between S and D contacts uniformly; hence the film should possess a single crystal-like morphology.

Among the organic semiconductor classes used in OFETs, (oligo, poly)thiophenes are among the most extensively investigated.[3a,6e−h,8,9] The first report of a polyheterocycle-based FET utilized a polythiophene,[10] with poly(3-hexyl)thiophene[11] and α,ω-dialkyloligothiophenes[12] being the first truly high-mobility polymeric and small molecule materials, respectively. Since then, chemical modification(s) of the thiophene core, variations in ring-to-ring connectivity and substitution pattern, have resulted in the synthesis and evaluation of a large number of thiophene-based materials.[9] However, with the recently reported exceptions of narrow classes of α,ω-di(cyanomethanide,[8e,f] perfluorohexyl,[8d] and perfluoroarene[8a])-substituted oligothiophenes (nTs), all of these materials are p-type semiconductors. Note that, despite the excellent performance, the dicyanomethanide class mentioned above better approximates an oligovinylene-like structure than an oligoheterocycle, due to the largely quinoid character of the ground state. Therefore, very little is known about the thin-film properties of n-type oligothiophenes and how/if their film microstructure and morphology

(6) (a) Kunugi, Y.; Takimiya, K.; Yamane, K.; Yamashita, K.; Aso, Y.; Otsubo, T. *Chem. Mater.* **2003**, *15*, 6. (b) Ponomarenko, S. A.; Kirchmeyer, S.; Elschner, A.; Huisman, B.-H.; Karbach, A.; Drechsler, D. *Adv. Funct. Mater.* **2003**, *13*, 591. (c) Afzali, A.; Dimitrakopoulos, C. D.; Breen, T. *J. Am. Chem. Soc.* **2002**, *124*, 8812. (d) Mitzi, D. B.; Dimitrakopoulos, C. D.; Kosbar, L. L. *Chem. Mater.* **2001**, *13*, 3728. (e) Dimitrakopoulos, C. D.; Malenfant, P. R. L. *Adv. Mater.* **2002**, *14*, 99. (f) Wurthner, F. *Angew. Chem., Int. Ed.* **2001**, *40*, 1037. (g) Dimitrakopoulos, C. D.; Mascaro, D. J. *IBM J. Res. Dev.* **2001**, *45*, 11. (h) Kraft, A. *ChemPhysChem* **2001**, *2*, 163.

(7) (a) Meng, H.; Bendikov, M.; Mitchell, G.; Holgeson, R.; Wudl, F.; Bao, Z.; Siegrist, T.; Kloc, C.; Chen, C.-H. *Adv. Mater.* **2003**, *15*, 1090. (b) Kunugi, Y.; Takimiya, K.; Yamane, K.; Yamashita, K.; Aso, Y.; Otsubo, T. *Chem. Mater.* **2003**, *15*, 6. (c) Videlot, C.; Ackermann, J.; Blanchard, P.; Raimundo, J.-M.; Frere, P.; Allain, M.; de Bettignies, R.; Levillain, E.; Roncali, J. *Adv. Mater.* **2003**, *15*, 306. (d) Halik, M.; Klauk, H.; Zschieschang, U.; Scmid, G.; Ponomarenko, S.; Kiechmayer, S.; Weber, W. *Adv. Mater.* **2003**, *15*, 917. (e) Ito, K.; Suzuki, T.; Sakamoto, Y.; Kubota, D.; Inoue, Y.; Sato, F.; Tokito, S. *Angew. Chem., Int. Ed.* **2003**, *42*, 1159. (f) Sandberg, H.; Henze, O.; Kilbinger, A. F. M.; Sirringhaus, H.; Feast, W. J.; Friend, R. H *Synth. Met.* **2003**, *137*, 885. (g) Meng, H.; Zheng, J.; Lovinger, A. J.; Wang, B.-C.; Van Patten, P. G.; Bao, Z. *Chem. Mater.* **2003**, *15*, 1778. (h) Kunugi, Y.; Takimiya, K.; Yamashita, K.; Aso, Y.; Otsubo, T. *Chem. Lett.* **2002**, *31*, 958.

(8) (a) Facchetti, A.; Yoon, M.-H.; Stern, C. L.; Katz, H. E.; Marks, T. J. *Angew. Chem., Int. Ed.* **2003**, *42*, 3900. (b) Katz, H. E.; Otsuki, J.; Yamazaki, K.; Suka, A.; Takido, T.; Lovinger, A. J.; Raghavachari, K. *Chem. Lett.* **2003**, *32*, 508−509. (c) Locklin, J.; Shinbo, K.; Onishi, K.; Kaneko, F.; Bao, Z.; Advincula, R. C. *Chem. Mater.* **2003**, *15*, 1404. (d) Facchetti, A.; Mushrush, M.; Katz, H. E.; Marks, T. J. *Adv. Mater.* **2003**, *15*, 33. (e) Chesterfield, R. J.; Newman, C. R.; Pappenfus, T. M.; Ewbank, P. C.; Haukaas, M. H.; Mann, K. R.; Miller, L. L.; Frisbie, C. D. *Adv. Mater.* **2003**, *15*, 1278. (f) Pappenfus, T. M.; Chesterfield, R. J.; Frisbie, C. D.; Mann, K. R.; Casado, J.; Raff, J. D.; Miller, L. L. *J. Am. Chem. Soc.* **2002**, *124*, 4184. (g) Yassar, A.; Demanze, F.; Jaafari, A.; El Idrissi, M.; Coupry, C. *Adv. Funct. Mater.* **2002**, *12*, 699. (h) Katz, H. E.; Johnson, J.; Lovinger, A. J.; Li, W. *J. Am. Chem. Soc.* **2000**, *122*, 7787. (i) Crone, B.; Dodabalapur, A.; Lin, Y. Y.; Filas, R. W.; Bao, Z.; LaDuca, A.; Sarpeshkar, R.; Katz, H. E.; Li, W. *Nature* **2000**, *403*, 521. (j) Heidenhain, So. B.; Sakamoto, Y.; Suzuki, T.; Miura, A.; Fujikawa, H.; Mori, T.; Tokito, S.; Taga, Y. *J. Am. Chem. Soc.* **2000**, *122*, 10240. (k) Facchetti, A.; Deng, Y.; Wang, A.; Koide, Y.; Sirringhaus, H.; Marks, T. J.; Friend, R. H. *Angew. Chem., Int. Ed.* **2000**, *39*, 4547. (l) Renak, M. L.; Bartholomew, G. P.; Wang, S.; Ricatto, P. J.; Lachicotte, R. J.; Bazan, G. C. *J. Am. Chem. Soc.* **1999**, *121*, 7787. (m) Bao, Z.; Lovinger, A. J.; Brown, J. *J. Am. Chem. Soc.* **1998**, *120*, 207.

(9) (a) Bäuerle, P. In *Electronic Materials: The Oligomer Approach*; Müllen, K., Egner, G., Eds.; Wiley−VCH: Weinheim, 1998; p 105. (b) Groenendaal, L.; Meijer, E. W.; Vekemans, J. A. J. M. In *Electronic Materials: The Oligomer Approach*; Müllen, K., Egner, G., Eds.; Wiley−VCH: Weinheim, 1998; p 235. (c) Moratti, S. C. In *Handbook of Conducting Polymers*, 2nd ed.; Skotheim, T. A., Elsenbaumer, R. L., Reynolds, J. R., Eds.; Marcel Dekker: New York, 1998; p 343. (d) Gruber, J.; Chia Li, R. W.; Hümmelgen, I. A. In *Handbook of Advanced Electronic and Photonic Materials and Devices*; Nalwa, H. S., Ed.; Academic: San Diego, CA, 2000; Vol. 8, pp 163−184. (e) Meng, H.; Zheng, J.; Lovinger, A. J.; Wang, B.-C.; Van Patten, P. G.; Bao, Z. *Chem. Mater.* **2003**, *15*, 1778. (f) Reddinger, J. L.; Reynolds, J. R. *Adv. Polym. Sci.* **1999**, *145*, 57. (g) McCullough, R. D. *Adv. Mater.* **1998**, *10*, 93.

(10) Tsumara, A.; Koezuka, H.; Ando, T. *Appl. Phys. Lett.* **1986**, *49*, 1210.

(11) (a) Sirringhaus, H.; Tessler, N.; Friend, R. H. *Science* **1998**, *280*, 1741. (b) Bao, Z.; Dodabalapur, A. J.; Lovinger, A. J. *Appl. Phys. Lett.* **1996**, *69*, 4108.

(12) (a) Akimichi, H.; Waragai, K.; Hotta, S.; Kano, H.; Sakaki, H. *Appl. Phys. Lett.* **1991**, *58*, 1500. (b) Garnier, F.; Yassar, A.; Hajlaoui, R.; Horowitz, G.; Deloffre, F.; Servet, B.; Ries, S.; Alnot, P. *J. Am. Chem. Soc.* **1993**, *115*, 8716.

affect electrical performance as compared to relationships established for the corresponding p-type systems. Furthermore, the mechanism underlying the "switch" from intrinsic p-type activity to n-type behavior in oligothiophenes and in other classes of electron-transporting materials is not understood.

In a closely related contribution,[13] we describe the synthesis of several broad classes of fluorocarbon-functionalized oligothiophenes **1** (DFH-nTs, $n = 2-6$) and **2** (isoDFH-nTs) and compare the molecular/solid-state properties with the corresponding fluorine-free alkyl-substituted **3** (DH-nTs, $n = 2-6$) and **4** (isoDH-nTs) and the parent unsubstituted oligothiophenes **5** (αnTs, $n = 2-6$). We demonstrate that all fluorocarbon-substituted oligothiophenes investigated have impressive chemical/thermal stability, volatility, and exhibit similar packing characteristics, strong $\pi-\pi$ intermolecular interactions, and comparable LUMO energies across the conjugation lengths. In preliminary work, it was shown that DFH-nTs ($n = 4-6$) are n-type semiconductors with mobilities, in the case of **DFH-4T**, as high as 0.04 $cm^2/(V\ s)$.[8d] Therefore, it is important to understand if the thin-film electrical properties of the remaining members of classes **1** and **2** correlate with the energetic positions of their frontier MOs[13] and are thus n-type transporting materials. Furthermore, because the FET performance of DFH-nTs ($n = 4-6$) has not been previously optimized, it may be possible to achieve even greater FET responses. Another fundamental question which is currently unanswered is whether **1** → **2** regiochemical modifications produce dramatic effects of the type recently communicated in the mixed perfluoroarene-thiophene series,[8a] where displacement of the fluorinated moiety from the molecular periphery to the core inverts the majority carrier sign from n- to p-type. Therefore, a priori, the carrier type of the β,β'-diperfluorohexyl-systems **2**, if active, might not be what is expected from simple consideration of relative HOMO and LUMO energies. To investigate these issues in greater depth, fluorocarbon-substituted sexithiophenes **6** (**iso2DFH-6T**) and **7** (**iso3DFH-6T**) were synthesized for the first time and investigated. These systems are ideal candidates for this study because now the perfluorohexyl chains are displaced progressively from the very end to the center of the π conjugated core (**DFH-6T** → **isoDFH-6T** → **iso2DFH-6T** → **iso3DFH-6T**).

Another interesting aspect of the present study involves the contrasting electrical properties of regiochemically pure β,β'-dialkyl substituted derivatives. End-capped alkyl-substituted oligothiophenes **3** have been extensively studied as semiconducting FET components and all exhibit p-type activity. However, β,β'-disubstituted oligothiophenes have been studied far less,[14] and the only report known to us concerns β,β'-dihexyl-substituted 6T, which exhibits poor performance.[12b] Therefore, it is important to determine if the reported lower mobilities of these systems are the result of the particular regiochemical substitution or whether the reported data were compromised by isomeric impurities/growth conditions.

In addition, such a large and diverse array of compounds offers the unique possibility of investigating the thin-film properties and TFT semiconducting behavior of broad oligothiophene families. Variations in oligomer dimension (from two to six thiophene units), substitution pattern (α vs β), and substituent electronic and lipophilicity characteristics (hexyl vs perfluorohexyl) provide an extensive group of molecular architectures to explore. One important question is how these variations in molecular parameters affect film growth morphology and microstructure and film electrical characteristics. **DFH-6T** is the first thiophene-based semiconductor to display n-channel mobility,[8k] and obviously this new phenomenon introduces many questions regarding electron versus hole transport within thiophene-based materials. With 27 compounds in hand that vary in conjugation length, substituent, and substitution position, it is now possible to analyze in depth trends in electrical and other properties, and to correlate them with molecular/solid-state structure. To our knowledge, there are no prior studies comparing the OFET response of p- and n-type semiconducting materials having the same core structure and prepared under identical film growth, device configuration, and environmental measurement conditions. From such studies, it should be possible to gauge important design motifs and thereby to envision next-generation materials for OFETs.

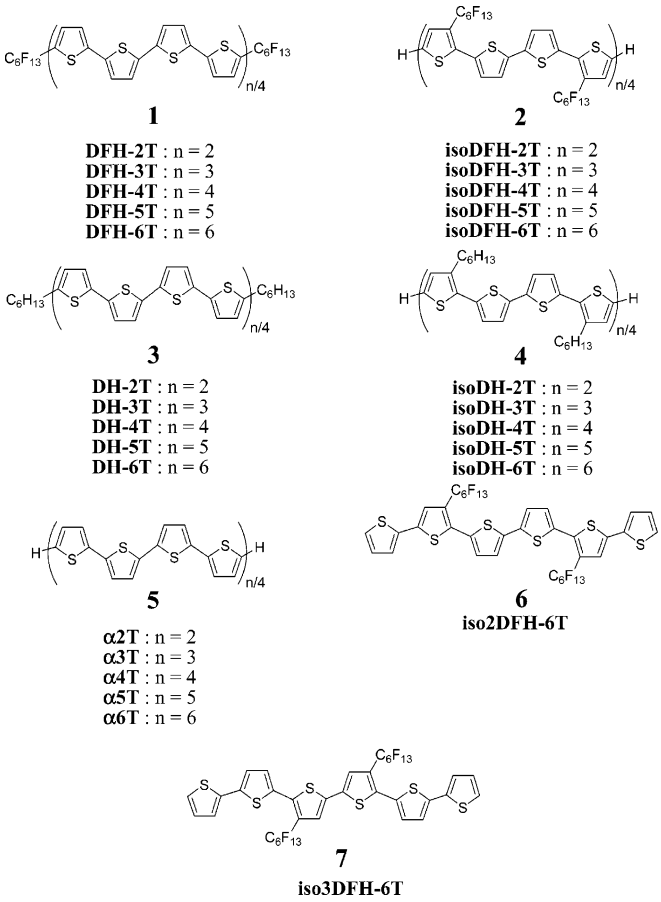

To achieve the aforementioned goals, the synthesis of new organic compounds was combined with thin-film growth/characterization, and device fabrication/electrical measurements. In particular, the comparative film microstructures and morphologies of **1**−**4**, **6**, and **7** were investigated by X-ray diffraction (XRD) and scanning electron microscopy (SEM). Our results indicate surprising similarities between film microstructural features of the different series and quantitative information on the relative molecular alignments. We show here via FET measurements that families **1** and **2** with the fluorocarbon chain on the thiophene termini and that alkyl- and

(13) Facchetti, A.; Yoon, M.-H.; Hutchison, G. R.; Stern, C. L.; Ratner, M. A.; Marks, T. J. *J. Am. Chem. Soc.*, in press.
(14) Barbarella, G.; Zambianchi, M.; Antolini, L.; Ostoja, P.; Maccagnani, P.; Bongini, A.; Marseglia, E. A.; Tedesco, E.; Gigli, G.; Cingolani, R. *J. Am. Chem. Soc*. **1999**, *121*, 8920.

Scheme 1. Synthesis of Compounds **6** and **7**

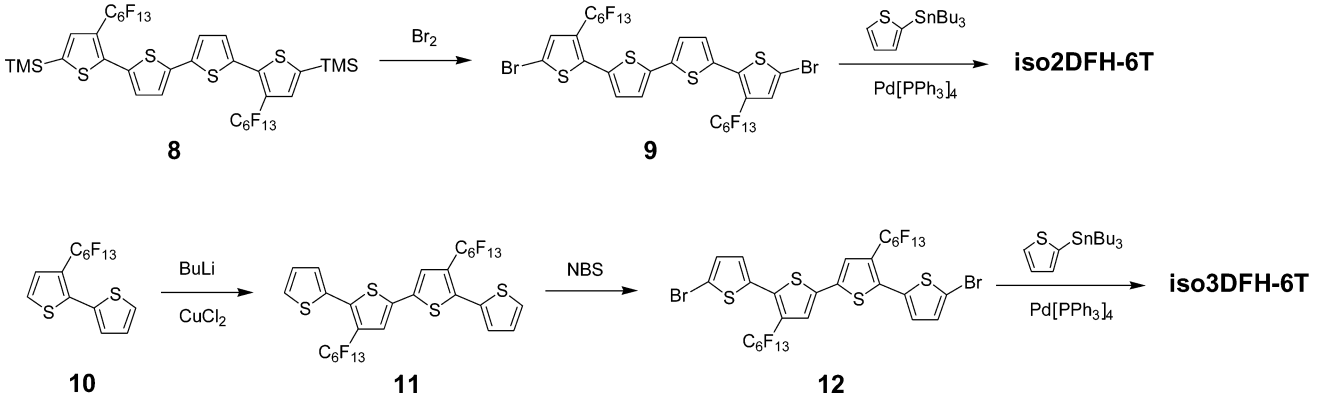

unsubstituted oligothiophenes **3**−**5** are rigorously distinct in terms of their semiconducting characteristics, with exclusively p- and n-type behavior, respectively, for all systems. On the other hand, the electrical response of **6** and **7** demonstrates the strategic influence of regiochemistry in formation of the majority carrier channel. These fascinating results stimulated us to study/analyze these materials with density functional theory calculations. A straightforward theoretical barrier modulation picture, supported by experimental data, provides an adequate, self-consistent explanation of the FET response and elucidates why small differences in molecular/film HOMO and LUMO energies of microstructurally similar compounds result in large changes in film electrical behavior and majority carrier sign.

Experimental Section

Materials. The reagents 5,5‴-bistrimethylsilyl-3,3‴-diperfluorohexyl-2,2′:5′,2″:5″,2‴-quaterthiophene, 3-perfluorohexyl-2,2′-dithiophene, and compounds **1**−**5** were prepared according to known procedures.[13]

3′,4″-Diperfluorohexyl-5,5‴-dibromo-2,2′:5′,2″:5″,2‴-quaterthiophene (8). Br_2 (0.20 g, 1.24 mmol) was added to a cold solution of 5,5‴-bistrimethylsilyl-3,3‴-diperfluorohexyl-2,2′:5′,2″:5″,2‴-quaterthiophene (0.62 g, 0.56 mmol) in chloroform (30 mL). The reaction mixture was stirred overnight at room temperature, and, after evaporation of the solvent, the residue was recrystallized from toluene−EtOH to afford the pure product as a yellow solid (0.50 g, 0.445 mmol, 79.5% yield). mp 130−133 °C. ^{1}H NMR ($CDCl_3$): δ 7.21 (2H, s), 7.02 (2H, d, $^3J = 4.0$), 6.96 (2H, d). ^{19}F NMR ($CDCl_3$): δ −81.30 (6F), −103.35 (4F), −121.26 (2F), −122.07 (4F), −123.18 (4F), −126.54 (6F). Anal. Calcd for $C_{28}H_6Br_2F_{26}S_4$: C, 29.91; H, 0.54; F, 43.93. Found: C, 30.12; H, 0.52; F, 43.88.

4″,3‴-Diperfluorohexyl-2,2′:5′,2″:5″,2‴:5‴,2⁗:5⁗,2⁗′:5⁗′,2⁗′′-sexithiophene (iso2DFH-6T). A mixture of 2-(tri-*n*-butylstannyl)-thiophene (0.54 g, 0.89 mmol), 3′,4″-diperfluorohexyl-5,5‴-dibromo-2,2′:5′,2″:5″,2‴-quaterthiophene (0.46 g, 0.41 mmol), and tetrakis(triphenylphosphine)palladium(0) (0.02 g, 0.015 mmol) in dry DMF (10 mL) was deareated twice with nitrogen. The reaction mixture was then heated at 85 °C overnight during which time a precipitate formed. After the precipitate was cooled, the bright yellow solid was collected and washed several times with methanol, hexane, and Et_2O to afford the pure product (0.41 g, 0.36 mmol, 87.9% yield). mp 165 °C (toluene). Anal. Calcd for $C_{36}H_{12}F_{26}S_6$: C, 38.24; H, 1.07; F, 43.68. Found: C, 38.14; H, 1.17; F, 43.61.

3′,4″-Diperfluorohexyl-2,2′:5′,2″:5″,2‴-quaterthiophene (11). Under nitrogen, *n*-BuLi (1.6 M, 6.45 mL) was added to a solution of 3-perfluorohexyl-2,2′-dithiophene (5.00 g, 10.32 mmol) in dry THF (60 mL) at −78 °C. After 1 h at this temperature, the dry ice bath was removed and the reaction mixture was stirred for an additional 20 min. Anhydrous $CuCl_2$ (3.39 g, 25.34 mmol) was then added, and the reaction mixture stirred overnight at 25 °C. Water (100 mL) was next added, and the solution was extracted with ether (3 × 80 mL). The organic phases ware collected, washed with water, and dried over $MgSO_4$. The solvent was removed to yield a solid that was chromatographed on silica gel (hexane) to afford the pure product as a light yellow solid (2.20 g, 2.28 mol, 44.2% yield). mp 135 °C (toluene−EtOH). ^{1}H NMR ($CDCl_3$): δ 7.41 (2H, d, $^3J = 5.13$), 7.23−7.18 (4H, m), 7.05 (2H, dd, $^3J = 3.7$). ^{19}F NMR ($CDCl_3$): δ −81.21 (6F), −103.32 (4F), −121.08 (4F), −122.18 (4F), −123.21 (4F), −126.54 (4F). Anal. Calcd for $C_{28}H_8F_{26}S_4$: C, 34.79; H, 0.83; F, 51.10. Found: C, 34.81; H, 0.97; F, 51.27.

5,5‴-Dibromo-3′,4″-diperfluorohexyl-2,2′:5′,2″:5″,2‴-quaterthiophene (12). *N*-Bromosuccinimide (0.302 g, 1.70 mmol) was added to a solution of 3′,4″-diperfluorohexyl-2,2′:5′,2″:5″,2‴-quaterthiophene (0.80 g, 0.83 mmol) in a DMF−$CHCl_3$ mixure (1:1, 20 mL) at room temperature. The reaction mixture was stirred overnight, during which time a precipitate formed. The $CHCl_3$ solution was next concentrated, and the precipitate was collected by filtration to afford the pure product as a yellow solid (0.91 g, 0.81 mmol, 97.6% yield). 124 °C (toluene−EtOH). ^{1}H NMR ($CDCl_3$): δ 7.20 (2H, s), 7.02 (2H, d, $^3J = 4.0$), 6.96 (2H, d). ^{19}F NMR ($CDCl_3$): δ −81.30 (6F), −103.35 (4F), −121.26 (2F), −122.07 (4F), −123.18 (4F), −126.54 (6F). Anal. Calcd for $C_{28}H_6Br_2F_{26}S_4$: C, 29.91; H, 0.54; F, 43.93. Found: C, 30.16; H, 0.72; F, 44.08.

3″,4‴-Diperfluorohexyl-2,2′:5′,2″:5″,2‴:5‴,2⁗:5⁗,2⁗′:5⁗′,2⁗′′-sexithiophene (iso3DFH-6T). A mixture of 2-(tri-*n*-butylstannyl)-thiophene (0.64 g, 1.71 mmol), 5,5‴-dibromo-3′,4″-diperfluorohexyl-2,2′:5′,2″:5″,2‴-quaterthiophene (0.80 g, 0.71 mmol), and tetrakis(triphenylphosphine)palladium(0) (0.02 g, 0.015 mmol) in dry DMF (15 mL) was deaerated twice with nitrogen. The reaction mixture was then heated at 85 °C overnight, during which time a precipitate formed. After the precipitate was cooled, a bright yellow solid was collected by filtration and washed several times with methanol, hexane, and Et_2O to afford the pure product (0.66 g, 0.58 mmol, 72.5% yield). mp 164 °C (toluene). Anal. Calcd for $C_{36}H_{12}F_{26}S_6$: C, 38.24; H, 1.07; F, 43.68. Found: C, 38.10; H, 1.23; F, 43.92.

Results and Discussion

Synthesis and Properties of Fluorocarbon-Substituted Sexithiophenes 6 and 7. New compounds **iso2DFH-6T** (**6**) and **iso3DFH-6T** (**7**) were targeted to study in detail regiochemistry effects on fluorocarbon-functionalized oligothiophenes. These systems can be conveniently synthesized according to Scheme 1. We previously described the preparation of key intermediates **8** and **10**.[13] Dibromo-derivative **9** was prepared directly in 80% yield by reaction of TMS-protected quaterthiophene **8** with a 10% stoichiometric excess of Br_2. Stille coupling of **9** with 2-tributylstannylthiophene affords **iso2DFH-6T** in 87% yield. The isomeric compound was prepared starting from 3-perfluorohexyl-dithiophene (**10**), which was lithiated and dimerized with $CuCl_2$ to afford diperfluorohexyl-4T (**11**) in 44% yield.

The subsequent bromination of **11** was accomplished quantitatively using NBS to afford **12**, which was reacted with 2-tributylstannylthiophene to give **iso3DFH-6T** in 72% yield.

The molecular properties of these oligothiophenes were investigated by optical spectroscopy and cyclic voltammetry. The UV−vis spectra and absorption maxima of **iso2DFH-6T** (387 nm) and **iso3DFH-6T** (388 nm) are significantly blue-shifted as compared to both **DFH-6T** (443 nm) and **isoDFH-6T** (420 nm), an indication of considerable inter-ring twisting. More importantly, the film spectra of **6** and **7** are considerably red-shifted as compared to those in solution (Figure S1), strongly suggesting the formation of J-aggregate-type structures. This behavior is opposite to that found not only in **DFH-6T** and **isoDFH-6T**, but also in all other fluorocarbon-functionalized nTs, where the film optical spectra suggest instead the formation of an H-aggregate-type structure. Therefore, solid-state structure and packing should be considerably different than in **1**−**5**. Cyclic voltammograms of **iso2DFH-6T** and **iso3DFH-6T** (THF solution, $TBAPF_4$ electrolyte) exhibit irreversible oxidative peaks at +1.49 and +1.44 V, respectively, and one-electron reversible reductions at −1.50 and −1.48 V, respectively, versus SCE. These reduction potentials are comparable to those of **DFH-6T** (−1.42 V) and **isoDFH-6T** (−1.50 V), arguing similar LUMO energy positions.

Film Morphology and Microstructure of 1−5. The films of longer oligomers ($n \geq 4$) were prepared by vacuum deposition. Because of lower melting points and greater volatility, films of smaller oligomers ($n = 2, 3$) were either cast from solution or evaporated in a small sublimer on a Schlenk line (vacuum < 1 Torr). The primary goal of X-ray film diffraction analysis here is to assess film microstructure and to determine the preferred molecular orientation of fluorocarbon-substituted films in comparison to that of alkyl-substituted and unsubstituted oligothiophenes. It is known that for organic TFT devices, charge transport is favored in the direction perpendicular to the long molecular axes (through conjugated cores of neighboring molecules);[9] thus a vertical alignment (in which molecular long axes are oriented perpendicular to the substrate surface) generally enhances transport properties.[15] The favorable microstructural alignment of many organic semiconductors is the key to their good FET performance. The following SEM investigation provides key information on film morphology because another requirement for good charge transport is either a continuous film (single-crystal like morphology) or large numbers of highly interconnected crystallites.

Single Crystal versus Polycrystalline Film XRD Analysis. Before discussing the XRD results for the oligothiophene films, it is useful to begin by correlating film X-ray $\theta-2\theta$ scan data for compounds of known crystal structure. This initial study allows a much more thorough analysis of the molecular ordering in these compounds. Single-crystal structures have been obtained for both **DFH-3T** [$Z = 8$, $a = 52.29$ Å, $b = 5.77$ Å, $c = 19.97$ Å, $\alpha = 90.00$, $\beta = 97.02$, $\gamma = 90.00$] and **DFH-4T** [$Z = 4$, $a = 61.10$ Å, $b = 5.75$ Å, $c = 8.97$ Å, $\alpha = 90.00$, $\beta = 94.50$, $\gamma = 90.00$], both of which crystallize in the space group $C2/c$.[13] Both compounds exhibit solid-state organization similar to that hypothesized for DH-6T[12b] and observed for members of the unsubstituted nT series,[16] with the oligothiophene cores and R^F substituents segregated in distinct regions. The overall structure is layered, with the molecular long axes aligned along the crystallographic *a*-axis. Within each individual layer, the molecules assemble in the well-known herringbone motif.[17] These crystal packing features are typical of molecules having a well-defined molecular long axis, for example, **α6T**[17] or 2,5-bis(4-biphenylyl)thiophene.[18]

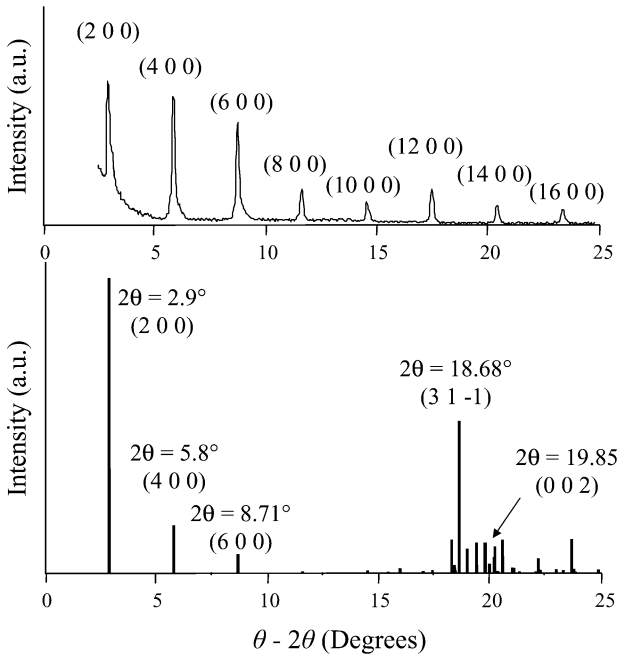

Figure 2. XRD $\theta-2\theta$ scan of a **DFH-4T** film grown at 70 °C (A), and a simulated powder pattern (B) with selected reflections labeled.

With crystal structure data in hand, it is straightforward to simulate powder patterns and therefore assign the reflections observed in the film XRD measurements. The reflections from the simulated (random crystallite orientation) powder patterns that can be readily identified in the $\theta-2\theta$ scans (2θ values, *d* spacings, relative intensities, and Miller indices) and the 2θ values of the experimentally observed reflections can be found in Tables S1−S3 (Supporting Information). Figure 2 illustrates a typical graphic comparison of experimental and simulated data, with a $\theta-2\theta$ scan for a **DFH-4T** film grown at elevated temperature (70 °C, A), and a **DFH-4T** powder pattern generated from the single-crystal data (B). The family of (*h* 0 0) reflections is particularly pronounced, from (2 0 0) to higher than (16 0 0). Note that the conditions for nonextinction in space group $C2/c$ are: (*h k* 0); $h + k = 2n$ and (0 0 *l*); $l = 2n$. Thus, reflections corresponding to (1 0 0), (3 0 0), and so on, with odd values of *h*, are not observed, as expected. The (2 0 0) reflection in the film XRD is observed at $2\theta = 3.0°$, corresponding to a *d* spacing of 29.4 Å, approximately one-half the length of the unit cell *a* axis. This set of (*h* 0 0) reflections is predominant, and even for **DFH-4T** films grown at room temperature, they are present, albeit weaker. This indicates that the films are highly textured and that the **DFH-4T** molecules in the thin films are predominantly aligned with their long molecular axes along the substrate normal, that is, that film

(15) (a) Fichou, D. *J. Mater. Chem.* **2000**, *10*, 571. (b) Horowithz, G. *J. Mater. Chem.* **1999**, *9*, 2021.

(16) Hotta, S.; Waragai, K. *Adv. Mater.* **1993**, *5*, 12.
(17) Siegrist, T.; Fleming, R. M.; Haddon, R. C.; Laudise, R. A.; Lovinger, A. J.; Katz, H. E.; Bridenbaugh, P.; Davis, D. D. *J. Mater. Res.* **1995**, *10*, 2170.
(18) Hotta, S.; Goto, M. *Adv. Mater.* **2002**, *14*, 498.

growth is favored in the *a* direction. It is also apparent that higher deposition/annealing temperatures make this *a*-directional alignment more favorable/ordered, as indicated by sharpening and increased intensity of the (*h* 0 0) reflections in $\theta-2\theta$ scans of the corresponding films.

One question that arises is the absence in the $\theta-2\theta$ scans of reflections belonging to (0 *k* 0) and (0 0 *l*). The lowest observable reflections (0 2 0) and (0 0 2) would be observed at $2\theta = 31.1°$ and 19.8°, respectively. These correspond to *d* spacings of 2.88 and 4.47 Å, or approximately one-half of the *b* axis and one-half of the *c* axis, respectively, of the unit cell. In fact, for some of the **DFH-4T** thin films, a weak peak at $2\theta = 19.8°$ for the (0 0 2) reflection is observed. As intensities vary from sample to sample, this reflection is not observed in $\theta-2\theta$ scans of some films, especially those exhibiting very strong (*h* 0 0) reflections, such as that shown in Figure 2. The (0 2 0) and (0 0 4) reflections are not observed in any of the samples. From the simulated powder pattern, intensities of the (0 2 0) and (0 0 4) reflections are predicted to be quite weak in a randomly oriented sample (see Table S1), and it is not surprising that they are not detected in the film XRD scans. Likewise, while the (0 0 2) reflection is predicted in the simulated powder pattern to be moderatly intense, the low intensity of this peak (or absence of it) in the film XRD of **DFH-4T** is in accord with the predominant ordering in the *a* direction.

A similar analysis can be carried out for **DFH-3T** films. Figure 3 shows a $\theta-2\theta$ scan for a film cast from solution with subsequent annealing (A) and a simulated powder pattern (C). Only one set of reflections, corresponding to the (*h* 0 0) family, is observed in the XRD. The (2 0 0) reflection appears at $2\theta = 3.4°$ and corresponds to a *d* spacing of 25.8 Å, which is approximately one molecular length, or one-half the distance of the unit cell *a* axis. As with **DFH-4T**, films of **DFH-3T** are highly textured and predominantly aligned with the molecular long axes oriented perpendicular to the substrate surface.

Microstructure details become more interesting for **DFH-3T** when the film is grown from the vapor phase at relatively high pressure (Schlenk line, $P < 1$ Torr) instead of cast from solution. Figure 3B displays the full scan, and the inset shows an enlarged view of the $2\theta = 2-15$ region. Reflections have been assigned on the basis of the simulated powder pattern. As with the solution-cast films, the (*h* 0 0) family of reflections is dominant for the sublimed film. The (5 1 0), (0 0 4), and (5 1 4) reflections at $2\theta = 17.6°$, 17.9°, and 26.0°, respectively, can be identified, although they are quite weak (Figure S2). The (0 0 4) reflection is predicted to have a significant intensity but is very weak in experimental film data and the (3 1 −2) reflection, predicted in the simulated random orientation powder pattern to be the most intense reflection for **DFH-3T**, is completely absent, in accord with the high degree of *a* axis preferential orientation. In Figure 3B, however, there is another distinct set of strong reflections that does not correlate with any predicted by the simulated powder pattern. This second strong set of reflections, marked with an asterisk, can be seen at 2θ values of 3.7°, 7.4°, 11.1°, 14.8°, 18.5°, 22.2°, and 29.8°. Thus, there are at least six higher-order reflections belonging to this set. Note that the simulated powder pattern represents all possible orientations of the crystallites; peaks that do not correlate with it must correspond to a different crystal structure. Thus, this dominant set of reflections corresponds to a different crystal structure or

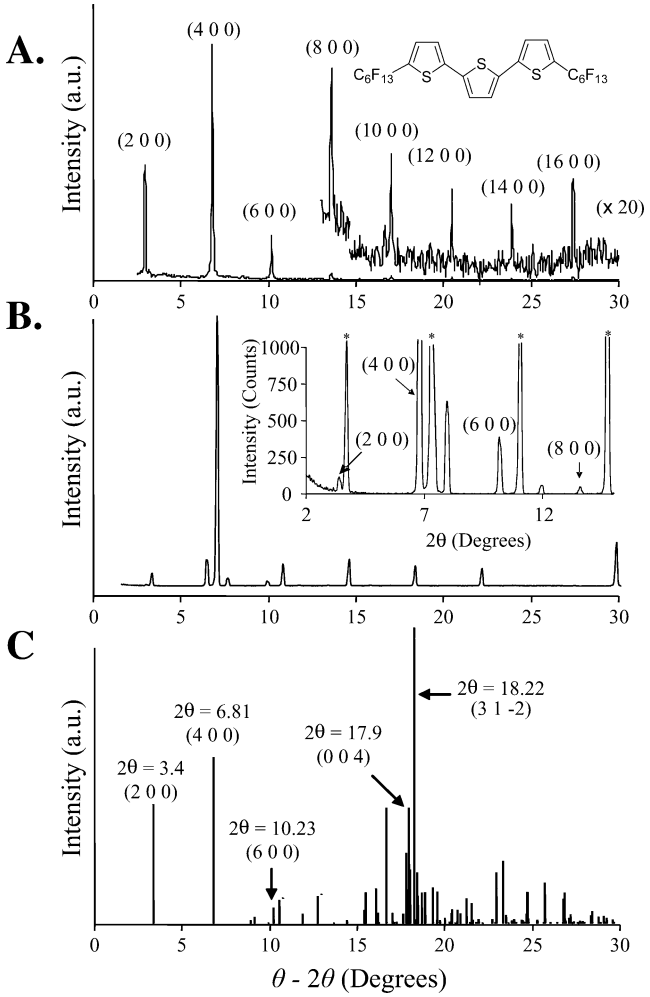

Figure 3. XRD $\theta-2\theta$ scan of a **DFH-3T** film. (A) Grown from solution and annealed. (B) Sample grown at ~1 Torr (inset expanded view). (C) Simulated powder pattern with selected reflections labeled.

polymorph of **DFH-3T** with an interlayer *d* spacing of 23.6 Å, slightly less than the *d* spacing of 25.8 Å observed for the (2 0 0) planes. Polymorphism has been observed for other classes of oligothiophenes as well.[15,19]

The availability of the **isoDFH-5T** crystal structure[13] provides additional insights into the film microstructure of oligothiophene series **2** and **4**. The unit cell of **isoDFH-5T** is triclinic (*P*1 space group) with the following parameters: $Z = 6$; $a = 10.4758$ Å, $b = 20.871$ Å, $c = 25.673$ Å; $\alpha = 79.45$, $\beta = 82.714$, $\gamma = 78.913$. Note that the conjugated thiophene backbones and the perfluorohexyl chains segregate as in the **DFH-3T** and **DFH-4T** structures.[13] The observed *d* spacing in the film is 25.1 Å ($2\theta = 3.5°$), which corresponds to the (0 0 *1*) reflection in the simulated powder pattern (Table S3, Figure S3). This distance is also equal to the length of the *c* axis of the crystal unit cell, implying that, as seen for **DFH-3T** and **DFH-4T**, molecules in the film are oriented with their long axes along the substrate normal. The (0 0 *l*) reflections have been assigned in the experimental spectrum, and higher-order reflections up to (0 0 9) are observed (note that there are no systematic absences predicted for space group *P*1). Thus, **isoDFH-5T** films are highly textured, with preferred growth having the crystallite *ab* faces parallel to the substrate surface. When **isoDFH-5T**

(19) Katz, H. E. *J. Mater. Chem.* **1997**, *7*, 369.

Table 1. Observed *d* Spacing Values and Computed/Experimental Geometric Parameters for Films of Compounds **1**−**5**

compound	*d* spacing (Å)	molecular length (Å)[a,b]
DFH-2T	23.1[c]	26.11
DFH-3T	25.9[c]	28.39 (29.23)
DFH-4T	29.4	32.43 (33.55)
DFH-5T	31.1	36.92
DFH-6T	36.1	40.77
isoDFH-2T		20.32
isoDFH-3T		20.17
isoDFH-4T	23.8[c]	28.14
isoDFH-5T	25.1[d]	29.94 (27.62)
isoDFH-6T	28.9	32.09
DH-2T	21.8[d]	25.99
DH-3T	27.3[d]	29.55
DH-4T	28.5	33.73
DH-5T	30	37.40
DH-6T	35.4	39.21
isoDH-2T		22.62
isoDH-3T		16.81
isoDH-4T		24.21 (24.16)
isoDH-5T	24.9	23.40
isoDH-6T	27.3	29.81
2T	7.82	10.90 (10.61, 10.90)
3T	13.05	14.82
4T	15.43	18.75 (18.17)
5T	19.45	22.67
6T	23.3	26.59 (26.14)

[a] Both lengths include standard van der Waals radii for carbon (1.70 Å), fluorine (1.50 Å), or hydrogen atoms (1.20 Å). [b] Numbers in parentheses indicate experimental values from X-ray crystal structures (see ref 13). [c] Sublimed (vacuum < 1 Torr) and annealed. [d] Grown at room temperature from solution. All other films were grown in the temperature range of 60−80 °C.

molecules are aligned in this manner on the substrate surface, the perfluorohexyl chains and the 5T core must be tilted at angles of 39−45° and 49°, respectively, with respect to the substrate normal.

***d* Spacing−nT Core Length Linear Correlations and Film Molecular Alignment.** Standard $\theta-2\theta$ XRD scans of DFH-/isoDFH-nT films grown in the temperature range of 60−80 °C, or for the shorter oligomers after annealing, display a very sharp low-angle reflection for all compounds and several higher-order reflections for many compounds as well (Figures 2, 3 and Figures S4, S5). Table 1 summarizes the observed *d* spacing values for **1**−**5**. Comparing **1** ↔ **3** and **2** ↔ **4** pairs, note that the *d* spacings of fluorocarbon-substituted DFH-/isoDFH-nTs are very similar (average difference is 0.9 Å) to those of the analogous alkyl-substituted DH-/isoDH-nT systems. Because the computed/experimental molecular lengths are also comparable between these series, this is an indication of similar film molecular orientations, independent of the chemical substitution. Note that the *d* spacing values are smaller than the molecular lengths, indicating an overall tilting of the long axes with respect to the substrate normal. Furthermore, with the exception of the **DFH**/**DH-3T** couple, the *d* spacings of the **1** and **2** series are larger than for the corresponding **3** and **4** series. At first glance, this difference might appear to originate from the greater steric requirements of fluorocarbon versus hydrocarbon chains. However, we demonstrate below that this is not the case.

Quantitative information on microstructure and molecular orientation for all **1**−**5** films is gained by plotting the observed *d* spacing values versus the thiophene core lengths (Figure 4). Note the good linearity of these plots for DFH-nTs ($y = 3.13x + 16.58$; $R^2 = 0.98$), DH-nTs ($y = 3.01x + 16.52$; $R^2 = 0.94$), and αnTs ($y = 3.74x + 0.87$; $R^2 = 0.99$). The observed linearity

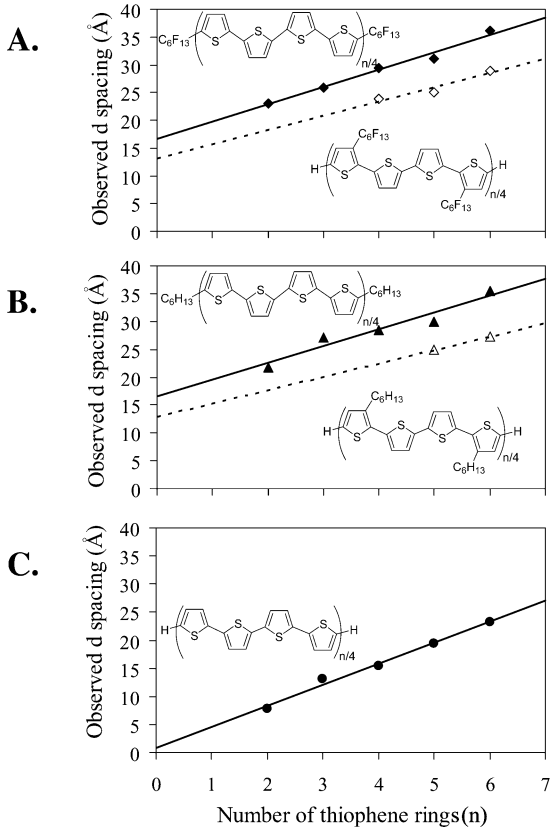

Figure 4. Plots of the observed film *d* spacings versus molecular core length expressed as the number of thiophene rings (n) for: (A) DFH-nTs (solid line) and isoDFH-nTs (broken line). (B) DH-nTs (solid line) and isoDH-nTs (broken line). (C) αnTs.

is striking evidence that within each series the molecules are oriented in a very similar manner independent of the core dimensions. The comparison between the **DFH-3T** and **DFH-4T** polycrystalline film and single-crystal XRD data demonstrates the growth of alternating layers of fluorocarbon and aromatic regions parallel to the substrate surface.[13] Therefore, similar lamellar microstructures are present for all fluorocarbon-substituted systems and, by extension in view of the similarities in molecular lengths, bond connectivities, and *d* spacings, to the corresponding DH-nT series (Figure 5). Furthermore, the intercept of these plots corresponds to the distance between alternating aromatic layers, which is the thickness along the substrate normal of the fluorocarbon/hydrocarbon region. From the crystal structures of **DFH-3T**/**-4T**[13] and alkyl-substituted oligothiophenes,[20] the lengths of the R^F and R^H chains are estimated as 9.07 and 8.40 Å, respectively, considering the van der Waals radii of F (1.50 Å) and H (1.20 Å). Therefore, the lengths of two linear and aligned perfluorohexyl (l_F) and hexyl (l_H) substituents are estimated to be 18.14 and 16.80 Å, respectively. Consequently, with respect to the substrate normal, the R^F and R^H chains should be tilted at an angle ϕ_{ch} given by $\cos^{-1}(16.58/18.16) = 24.1°$ and $\cos^{-1}(16.52/16.80) = 10.5°$, respectively. However, the former value appears to be considerably larger than the tilt angle of the fluorocarbon chains with respect to the *bc* plane normal found in the crystal structures of **DFH-3T** (6−9°) and **DFH-4T** (4−5°).[13] To determine the conformation of the fluorocarbon-substituted systems precisely,

(20) Destri, S.; Ferro, D. R.; Khotina, I. A.; Porzio, W.; Farina, A. *Macromol. Chem. Phys.* **1998**, *199*, 1973.

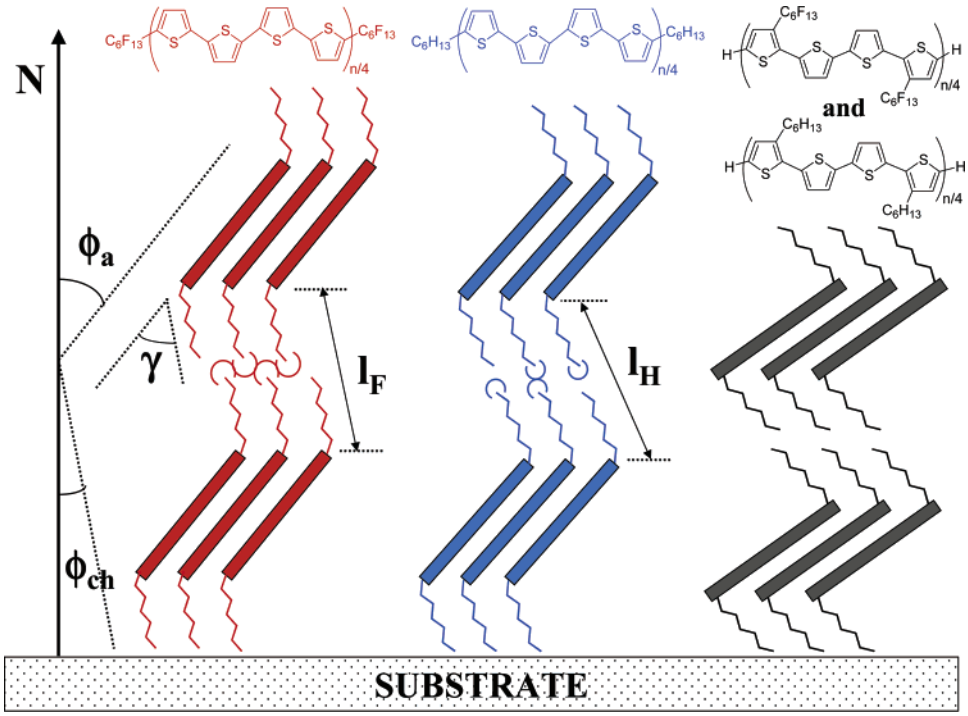

Figure 5. Schematic molecular growth orientations of films of **1**−**4** on Si/SiO_2 substrates.

note that the actual l_F value is slightly shorter than twice the actual R^F length. Unlike hydrocarbons,[21] fluorocarbon chains do not pack with two high electron density trifluoromethyl groups directly facing each other, but rather with one slipped with respect to the other, with the end-CF_3 slightly intermingled by a depth of approximately the fluorine van der Waals radius (see Figure 5). Such a relative arrangement of R^F substituent chains has been observed previously not only in the crystal structures of our perfluorohexyl-oligothiophenes[13] but also in other systems such as fluorocarbon-substituted NTCDI[22] and benzenoid systems.[23] Therefore, the correct length (thickness) of two slipped, slightly interdigitated fluorocarbon substituents should be ∼(18.14−1.50) = 16.66 Å and the R^F tilt angle for the DFH-nT series should be ∼6°, in excellent agreement with the average values found solely from the crystal structures of **DFH-3T** and **DFH-4T**. Of particular importance here also is the slope of the plots in Figure 4, which can be assumed to represent the increase of *d* spacings in series **1** (3.13), **3** (3.01), and **5** (3.74) upon extension of the core by one thiophene ring. Comparing these values with the corresponding length of thiophene (3.9 Å),[13] it can be concluded that the *ipso*C−*ipso*C vector of the rigid aromatic unit tilts with respect the substrate normal by ∼37° (**1**), 40° (**3**), and 17° (**5**), independent of the core dimension! Note that the former two values differ slightly but are considerably larger than the tilt angle found for αnTs (**5**), and the reported ϕ_a value for α,ω-dimethyl-4T films is (∼26°).[24] Therefore, it appears that while variation in the thiophene core extension has little influence on ϕ_a, the length of the substituent does, with an increase of the core tilt angle with increased substituent length. The combination of these results leads to three important conclusions: (i) DFH-nT and DH-nT films deposited in the substrate temperature range 60−80 °C are microstructurally very similar and therefore the crystal structures of these systems, if/when obtained, should reflect these similarities in molecular packing, orientation, and geometry. (ii) The larger observed *d*-spacings for the DFH-nT films as compared to DH-nTs are not the result of the larger F versus H van der Waals radii, but rather are due to the smaller tilt angles of both core and substituents in DFH-nT versus DH-nT films. (iii) Combining ϕ_{ch} with ϕ_a, it is also possible to compute the average relative angle ($\gamma = \phi_{ch} + \phi_a$) between the core and the chains (Figure 5). This angle, which originates in the packing of segregating fragments (core and chains) and minimization of free volume in the solid,[25] is found to be 42.2° and 50.2° for DFH-nT and DH-nT films, respectively. The former value is in excellent agreement with the **DFH-3T** and **DFH-4T** crystal structures, whereas the latter is considerably greater than that reported by Garnier et al. for **DH-6T** (16°) in a seminal paper on oligothiophene semiconductors.[12b] A possible explanation for this discrepancy could be a previous underestimation of the 6T core length (20.2 instead of 22.4 Å)[17] and the uncertainty in the actual distance between hexyl−hexyl chains and 6T−6T cores in **DH-6T**, because the crystal structure is unknown.

When the plots of isoDFH-nT ($y = 2.55x + 13.18$; $R^2 = 0.93$) and isoDH-nT ($y = 2.40x + 12.90$; $R^2 = 1.00$) *d* spacings versus n are considered (Figure 4), the smaller number of experimental points significantly reduces precision in the linear correlations. Nevertheless, meaningful film microstructural information can be obtained. First, the reduced values of both intercepts and slopes as compared to the other oligothiophenes indicate much larger tilt angles for both substituents [$\phi_{ch} = \sim 38°$ (isoDFH-nTs), ∼40° (isoDH-nTs)] and cores [$\phi_a \approx 49°$ (isoDFH-nTs), ∼52° (isoDH-nTs)]. These data are in excellent agreement with the crystal structure of **isoDFH-5T** and with

(21) Pauling, L. *The Nature of the Chemical Bond*; Cornell University Press: New York, 1962.
(22) Katz, H. E.; Siegrist, T.; Schon, H. J.; Kloc, C.; Batlogg, B.; Lovinger, A. J.; Johnson, J. *ChemPhysChem* **2001**, *3*, 167.
(23) Krebs, F. C.; Spanggaard, H. *J. Org. Chem.* **2002**, *67*, 7185.
(24) Hotta, S.; Waragai, K. *J. Mater. Chem.* **1991**, *5*, 835.
(25) Weber, P.; Guillon, D.; Skoulios, A. *Liq. Cryst.* **1991**, *3*, 369.

that of β,β'-dialkyl-substituted quaterthiophenes.[26] Second, the lamellar microstructure is preserved in all films despite the dramatic changes in molecular geometry. Third, ϕ_a in isoDFH/isoDH-nT films is large, and the effective thickness of each molecular core channel for charge transport (obtained from projection of the core length on the substrate normal) is greatly reduced with respect to the unsubstituted and α,ω-disubstituted compounds. This should adversely affect, in concomitance with decreases in the core conjugation, charge mobility in the corresponding films.

Film Microstructure versus Deposition Temperature. DFH-6T film microstructure was evaluated previously by XRD for a wide range of deposition temperatures.[8h] While the highest degree of texture (as inferred from the sharpest and maximum number of reflections of one dominant family in the $\theta-2\theta$ scan) results from quite high deposition temperatures (>200 °C), the best TFT device performance (defined as having the highest mobility and on/off ratio) is observed for films grown in the range ~80−100 °C. Thus, the growth conditions that lead to the greatest mobilities and on/off ratios are not necessarily correlated with the greatest texturing. Film morphology also plays an important role, as discussed in the next section. Films of **1**−**4** grown at room temperature, at various other substrate temperatures, and at room temperature with subsequent annealing were analyzed by XRD. Comparison of these $\theta-2\theta$ scans brings some important similarities/differences to light: (1) For room-temperature depositions, films of all fluorinated compounds exhibit weaker/broader and fewer reflections in the XRD spectra than the corresponding fluorine-free systems. (2) For all systems, peak sharpness and number of observed higher-order reflections generally increases with increasing deposition/annealing temperature, reach a maximum, and then decrease. (3) Annealing of room-temperature deposited films of **1** and **2** has the same effect on the XRD as using a higher deposition temperature during growth. The same effects are observed for the alkyl-substituted families, but require higher deposition temperature and/or longer annealing times. These observations indicate that the film deposition temperature should have much greater impact on the electrical properties of the fluorinated than for the fluorine-free films.

Compound **isoDFH-6T** is a representative example of the pronounced growth temperature sensitivity of film microstructure. Films of this system were grown over a wide range of temperatures (25, 50, 75, 100, and 125 °C) at the same growth rate, and the resulting microstructures were compared by XRD (Figure 6) and SEM (vide infra). For depositions at room temperature, the film is poorly textured, but at slightly higher deposition temperatures, a distinct set of reflections grows in, reaching the greatest sharpness (narrowest line widths) near 75 °C. At the highest temperatures (100 and 125 °C), these reflections broaden slightly, and a very broad feature appears around $2\theta = 15°$. It appears that the highest degree of texture occurs at a deposition temperature of ~75 °C, with deposition temperatures above and below this value affording less textured films. Correlation of these XRD data with SEM images allows us to reasonably predict and understand the range of deposition temperatures that will afford films with the highest mobilities and on/off ratios.

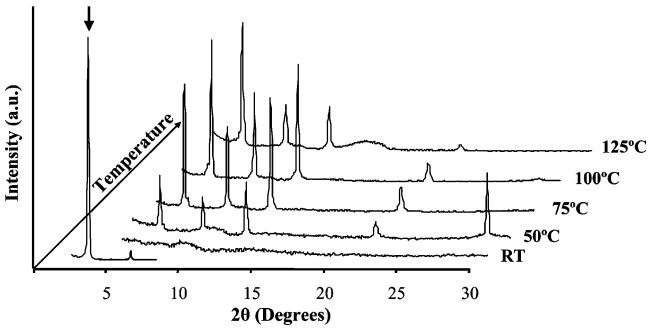

Figure 6. X-ray diffraction $\theta-2\theta$ scans of **isoDFH-6T** films of identical thickness grown at various substrate temperatures. The intense peak at 3.20 (indicated by an arrow) present in all spectra is omitted from the higher temperature data for ease of viewing.

Scanning Electron Microscopy. Morphological Investigation. The XRD $\theta-2\theta$ scans of films of **1**−**4** show that these compounds are all highly textured when grown (or annealed in the case of **1** and **2**) at ~60−80 °C. Because FET performance exhibits significant variation with growth temperature (vide infra), film morphology must also be considered in interpreting electrical performance. As previously observed in an SEM morphological study of **DFH-6T** films[8k] and other organic semiconductors,[6−8] the highest carrier mobility is obtained for films having the appropriate balance of large grain size and space-filling grain connectivity. SEM micrographs of **DFH-4T**, **DFH-5T**, and **DFH-6T** films grown at 70 °C (Figure S6) show that, although these films appear to have grains of approximately the same size, the **DFH-6T** film is less smooth, and discontinuities at grain boundaries can be readily observed. The films of **DFH-4T** and **DFH-5T**, in contrast, exhibit very smooth surfaces with fewer observable features. Under these growth conditions, **DFH-4T** and **DFH-5T** films exhibit electron mobilities an order of magnitude greater than that of **DFH-6T**.[8d] The less continuous and rougher morphology observed in films of the latter supports this trend. Interestingly, a similar phenomenon has been observed for the **DH-nT** series. The greater hole mobility observed for optimized films of **DH-4T** as compared to those of the larger **DH-5T** and **DH-6T** molecules has been attributed to the morphology at 80−100° growth temperatures, characterized by flat, lamellar crystallites (>10 μm in length) that are highly interconnected.[27] In addition, it has been shown that α,ω-alkyl substituted oligothiophenes exhibit significantly improved packing (as observed by X-ray diffraction) in comparison to their unsubstituted analogues.[12b] Thus, it is reasonable to suggest that the increasing relative contribution of the α,ω-substituents in DFH-nTs and DH-nTs with decreasing n (6 → 4) contributes to the smoother and more closely interconnected morphology observed in films of the smaller oligomers **DH-4T** and **DFH-4T**.

The effect of deposition temperature on film morphology is also evident in the case of **isoDFH-6T**, where films were grown at five different substrate temperatures ranging from 25 to 125 °C. The XRD $\theta-2\theta$ scans corresponding to these films are illustrated in Figure 6, while Figure 7 shows scanning electron micrographs of the same films. The micrographs are at the same magnification for ease of comparison. When deposited at room temperature, films of **isoDFH-6T** consist of very small grains

(26) Azumi, R.; Gotz, G.; Debaerdemaeker, T.; Bauerle, P. *Chem.-Eur. J.* **2000**, *6*, 735.

(27) (a) Katz, H. E.; Lovinger, A. J.; Laquindanum, J. G. *Chem. Mater.* **1998**, *10*, 457. (b) Dimitrakopoulos, C. D.; Furman, B. K.; Graham, T.; Hegde, S.; Purushothaman, S. *Synth. Met.* **1998**, *92*, 47.

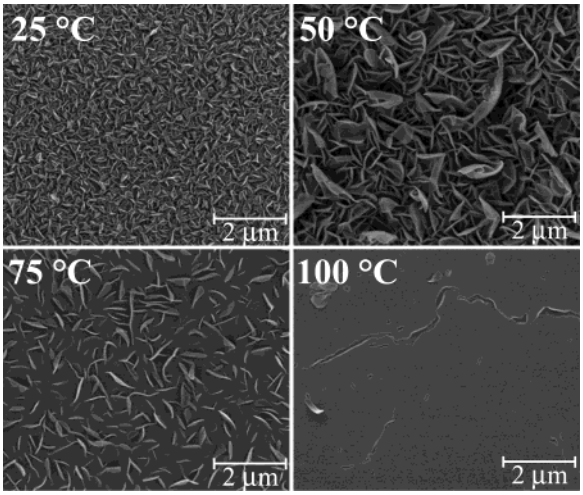

Figure 7. Scanning electron micrographs of **isoDFH-6T** films deposited at the indicated substrate temperatures.

that appear to have many ridges and gaps. When the deposition temperature is increased to 50 °C, the grains are considerably larger, although there still appear to be deep gaps and cavities within the branched structure. Deposition at 75 °C marks the onset of grain coalescence, and the film is very smooth with fewer and smaller grains protruding from the surface. The higher deposition temperature of 100 °C leads to a completely smooth film surface, but this is accompanied by the formation of pits or long cracks. At higher deposition temperatures (not shown), large leaflike protrusions from the smooth surface can again be observed (as at 75 °C), but there are still some cracks as well as large clusters of these leafy grains. In comparing these micrographs, it appears that the optimum combination of grain size and smooth interconnectedness lies, for this system, in a temperature range that is lower than 100 °C but not lower than 70 °C.

It will be shown (vide infra) that **isoDFH-6T** films exhibit mobilities more than 1 order of magnitude greater than those of **isoDFH-5T** films (both grown at 70 °C). Because films of both compounds are highly textured, as indicated by XRD $\theta-2\theta$ scans, morphology also likely plays a significant role in the observed differences in TFT performance. Indeed, SEM micrographs of **isoDFH-5T** films (70 °C) exhibit large cracks, and, at higher magnifications, it is evident that the film is composed of isolated, circular features (Figure 8A,B). With such discontinuities, the film morphology of **isoDFH-5T** is much less favorable for efficient charge transport than the smooth morphology seen in **isoDFH-6T** films grown in the same temperature range. The remaining β,β'-disubstituted compound, **isoDFH-4T**, was cast from solution (due to its high solubility and volatility) and examined by SEM. The films (Figure S7) appear to be extremely smooth with large, rounded features. As in the case of evaporated **isoDFH-5T** films, solution-cast **isoDFH-4T** films exhibit a sharp set of reflections in the XRD. Thus, it is a reasonable prediction based on the SEM that these films will have higher electron mobilities than films of **isoDFH-5T**/**6T**. For comparison, Figure 8C,D shows a SEM of an **isoDH-6T** film grown at 70 °C. It appears to be much smoother than the films of both **isoDFH-6T** and **isoDFH-5T**, although the grains on the surface are smaller. Electrical properties are discussed below. Finally, it is interesting to note that the difference (0.2 Å) in *d* spacing values for films of **isoDFH-5T**

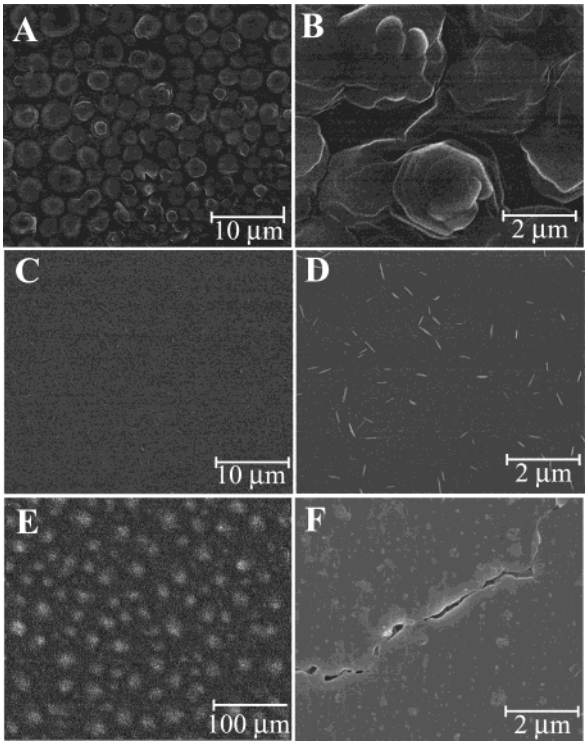

Figure 8. Scanning electron micrographs of: **isoDFH-5T** (A, B), **isoDH-6T** (C, D), and **isoDH-5T** (E, F) films deposited at a substrate temperature of 70 °C (at different magnifications).

and **isoDH-5T** is the smallest among the two series, leading to the reasonable assumption that they pack in a similar way. Note, the circular features observed for **isoDFH-5T** films are seen in **isoDH-5T** films as well (Figure 8E,F). In comparison to **isoDFH-5T**, these round features are much larger, although they still appear to be isolated or nearly isolated from each other on the substrate surface. A reasonable prediction is that **isoDH-5T** films will have much lower mobilities than **isoDH-6T** films; this would follow the same trend observed for **isoDFH-5T** and **isoDFH-6T**.

Field-Effect Transistors. Field-effect transistor devices were fabricated for all compounds of series DFH-nT (**1**) and DH-nT (**3**) ($n = 3-6$), isoDFH-nT (**2**) and nT (**5**) ($n = 4-6$), and isoDH-nT (**4**) ($n = 5, 6$) using the top-contact configuration (Figure 1). Most of these semiconductors were vacuum-deposited on top of HMDS-treated Si/SiO_2 substrates maintained at temperatures (T_D) of 25 and 70 °C. These two deposition temperatures were chosen from a balance between the results from the XRD/SEM investigations and consideration of the thermal properties (melting points, volatility characteristics) of the compounds. To show the precision of each measurement, the reported data are an average of at least three devices tested at different regions of the semiconductor layer. The electrical measurements were performed under vacuum ($\sim 10^{-5}$ Torr). Figure 9 shows typical drain−source current/voltage plots of two n- and p-type semiconductors operating at different gate biases, and exhibiting substantially different performance.

For purposes of comparison with other organic FETs, the mobilities were calculated by standard field-effect transistor equations. In conventional metal−insulator−semiconductor FETs (MISFETs), there is typically a linear and saturated regime in the I_{DS} versus V_{DS} plots for different V_G values. At large

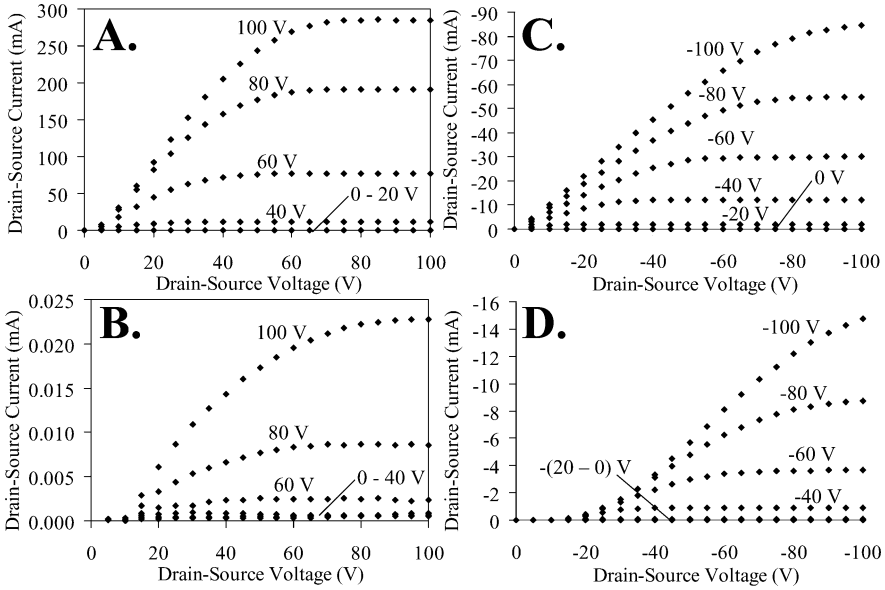

Figure 9. Drain−source current−voltage plots of: (A) **DFH-4T**, (B) **isoDFH-6T**, (C) **DH-4T**, and (D) **isoDH-6T** at different gate biases.

Table 2. FET Mobilities (μ, $cm^2\ V^{-1}\ s^{-1}$), Current On:Off Ratios (I_{on}:I_{off}), and Threshold Voltage (V_T, V) for Semiconductor Films of Series **1**−**5**

		25 °C			70 °C		
film	type	μ	I_{on}:I_{off}	V_T	μ	I_{on}:I_{off}	V_T
DFH-3T[a]	n	$\sim10^{-6}$	10^2	∼40	1×10^{-5}	5×10^2	20−30
DFH-4T	n	0.0004	10^3	∼40	0.059	2×10^5	25−30
DFH-5T	n	7×10^{-5}	10^2	∼70	0.026	6×10^4	35−40
DFH-6T	n	$\sim10^{-6}$	10^2	∼60	0.001	10^4	35−42
isoDFH-4T[b]	n	$\sim10^{-6}$	10^2	∼60	$\sim10^{-6}$	10^2	∼60
isoDFH-5T	n	8×10^{-5}	10^3	∼65	4×10^{-5}	10^3	∼60
isoDFH-6T	n	0.0003	10^3	∼70	0.0005	5×10^3	60−70
DH-3T[a]	p	0.0002	3×10^4	−0.35	0.0004	4×10^4	−3
DH-4T	p	0.061	10^6	−10	0.038	10^6	−3
DH-5T	p	0.051	10^4	−2	0.054	10^4	−12
DH-6T	p	0.044	2×10^3	−2	0.064	3×10^3	3
isoDH-5T[b]	p	0.0095	2×10^5	−20	0.012	4×10^5	−18
isoDH-6T	p	0.025	3×10^3	−6	0.064	7×10^3	−7
4T	p	0.011	10^5	−17	0.014	10^5	−15
5T	p	0.016	10^4	−2	0.036	10^5	−3
6T	p	0.039	2×10^4	−14	0.060	4×10^4	−12

[a] Film were prepared from solution. [b] 70 °C values refer to room-temperature vacuum-deposited film after annealing at 70 °C.

V_{DS}, the current saturates and is given by eq 1 where L and W are the device channel length and width

$$(I_{DS})_{sat} = (WC_i/2L)\mu(V_G - V_t)^2 \quad (1)$$

respectively, and C_i is the capacitance of the insulator (2×10^{-8} F/cm^2 for 300 nm SiO_2). The mobility and the threshold voltage (V_t) can then be calculated from the slope and intercept, respectively, of the linear portion of the V_G versus $(I_{sd})^{1/2}$ plot (at $V_{DS} = -100$ V). Table 2 collects the electrical data in terms of majority carrier sign, mobility, current on/off ratio, and V_t for all devices fabricated from compounds **1**−**5**. The comparative analysis of the electrical response/behavior obtained under stringently identical conditions reveals interesting similarities/differences between the fluorinated series and the other oligothiophenes, and within each series. The evaluation of these response characteristics and the underlying information they convey would have been extremely difficult to uncover employing available literature FET data for compounds **3** and **5**.

The first observation is that all of the semiconductors investigated are FET-active, independent of the chemical substitution, regiochemistry, and core dimension. Remarkably, the short oligomers **DFH-**/**DH-3T** also exhibit FET responses, despite the small conjugation length. Before considering the results on compounds **6** and **7**, note that all fluorocarbon-substituted systems functionalized at the terminal thiophene units (**1** and **2**) are n-type semiconductors, in contrast to the uniformly p-type activity exhibited by the remaining systems **3**−**5**. For all systems, the effect of increasing deposition temperature is generally to increase both μ and I_{ON}/I_{OFF} and to decrease V_t. Particularly interesting is the markedly different sensitivity of the carrier mobility to T_D for the fluoroalkyl- versus the alkyl- and unsubstituted oligothiophenes. For the latter systems, mobilities remain in a narrow range with a maximum variation on going from 25 to 70 °C of ∼2×. Similar variations over comparable T_D ranges have also been observed for **DH-4T**,[27a] **DH-5T**,[28] and **α6T**[29] in other studies, although the absolute

(28) Katz, H. E.; Lovinger, A. J.; Laquindanum, J. G. *Chem. Mater.* **1998**, *10*, 633.
(29) Servet, B.; Horowitz, G.; Ries, S.; Lagorsse, O.; Alnot, P.; Yassar, A.; Deloffre, F.; Srivastava, P.; Hajlaoui, R.; Lang, P.; Garnier, F. *Chem. Mater.* **1994**, *6*, 1809.

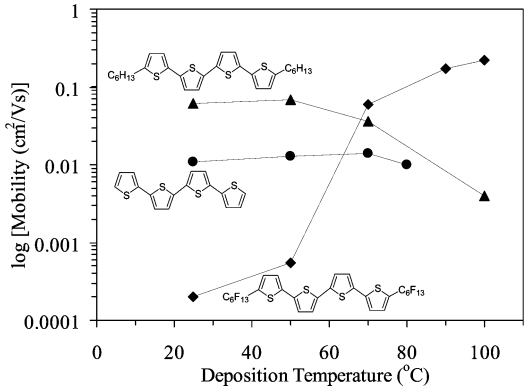

Figure 10. FET charge carrier mobilities of oligomers **DFH-4T** (◆), **DH-4T** (▲), and **α4T** (●) as a function of deposition temperature.

mobility values vary remarkably considering the different film growth/device experimental conditions. In marked contrast, DFH-/isoDFH-nTs exhibit much larger mobility variations, in some cases approaching 3 orders of magnitude.

Because **DFH-4T** films exhibit the highest n-type mobility among systems **1** and **2** for $T_D = 70$ °C (see Table 2), the growth temperature dependence of the mobility was explored in more detail for this system and, for comparison, for the corresponding **DH-4T** and **α4T** materials. The results are plotted in Figure 10, which shows that the mobilities of **DH-4T** and **α4T** remain in the range of ~0.05 and ~0.01 $cm^2/(V\ s)$, respectively, whereas the **DFH-4T** mobility increases from $\sim 10^{-4}$ ($T_D = 25$ °C) to 0.22 $cm^2/(V\ s)$ for film growth at 100 °C. To our knowledge, this is the highest n-type mobility ever reported for an n-type organic FET employing SiO_2 as the dielectric material. The difference between the performance of DFH/isoDFHnTs and the other systems as well as the dependence of μ on T_D are in line with the aforementioned morphology and microstructure properties of the corresponding films. For room-temperature depositions, DH-/isoDHnT films are already highly textured and quite smooth, and increases in the deposition temperature have a relatively minor influence on this favorable film microstructure. In the case of **DH-4T**, a decrease in mobility with increasing T_D is observed, in accord with the results of Katz et al.,[27a] probably due to formation of cracks in the films. The films of the unsubstituted oligothiophene αnTs are known to have a less favorable molecular alignment than the corresponding DH-nTs when deposited at room temperature.[12b] αnT films are composed of small (50−100 nm) highly interconnected crystallites with moderately smooth surfaces.[28,30] As the deposition temperature is increased, the net molecular orientation and crystallite size become more favorable for charge transport and, consequently, the mobility increases, on average, more than in the case of the alkyl-substituted analogues. For the present fluorinated series, films deposited at room temperature are less crystalline than those of the alkyl-substituted systems, and the morphology consists of very small (30−60 nm), poorly interconnected crystallites. The effect of the increased deposition temperature is to improve film texturing, to drastically enlarge crystallite dimensions, and to enhance crystal-to-crystal interconnections. This dramatic change in film microstructure with deposition temperature is confirmed by the effects of annealing DFH-nT films. For example, devices fabricated from **DFH-4T** films deposited at 25 °C with $\mu \approx 10^{-4}$ exhibit a mobility of ~0.01 $cm^2/(V\ s)$ after annealing at 100 °C for 15 min (before Au S−D deposition). Such extensive film microstructural reorganization at relatively low temperatures and short annealing times, which is not observed for **3**−**5** and other organic semiconductors,[31] is probably the consequence of the greater volatility/chain motion of the fluorocarbon chains. Due to the small fluorine atomic radius, large electronegativity, low polarizability, and large fluorine−fluorine repulsive energies, fluorocarbon chains undergo diffusional translation more readily than comparable hydrocarbon chains as is evident in the thermal behavior and temperature-dependent changes in crystallinity of many fluorinated materials and polymers, including PTFE.[32]

Differences in the V_t and $I_{on}:I_{off}$ data also underscore differences in chemical structure and transport characteristics between the fluorinated and fluorine-free oligothiophene series. V_t values of the DFH/isoDFH-nT films are always considerably larger than those of the other systems, meaning that electron injection has a greater overall barrier than hole injection. Such behavior has been observed for other n-type organic semiconductors.[8] Note that **DH-6T** has a positive V_t, meaning that at $V_G = 0$ V, there are already large numbers of free carriers and the device is already on. This behavior is suggestive of extensive environmental doping[33] and has important consequences for device current on/off ratios. Indeed, with the exception of the **DH-4T**/**DFH-4T** pair, the devices fabricated from the fluorinated nTs grown at 70 °C exhibit larger $I_{on}:I_{off}$ ratios despite the comparable/lower mobilities (see Figure 11 for comparative transfer plots of **DFH-**/**DH-4T** and **DFH-**/**DH-5T** couples). This means that, in general, the DFH/isoDFH-nTs have lower off currents than observed in the other systems, and consequently environmental doping is not as important in these series. Additional evidence for this mechanism is that semiconducting films of DFH/isoDFH-nTs left in air for more than 1 month still exhibit off currents in the range of 10^{-10}−10^{-11} A at $V_{SD} = 100$ V (for device dimensions, see Experimental Section). In contrast, identical DH-nT/isoDH-nT-based devices stored under the same conditions exhibit far larger I_{DS} currents (10^{-6}−10^{-9} A), clearly demonstrating that the effect of fluoroalkyl substitution is not only to invert the majority carrier sign for all oligomers, but also to inhibit environmental doping. The case of **DH-4T** is particularly instructive because reduction of the core size is known to greatly inhibit self-doping in fluorine-free systems,[34] and the corresponding devices (freshly fabricated) exhibit very low initial currents ($\sim 10^{-11}$) and, consequently, very large $I_{on}:I_{off}$ ratios.

Especially interesting here are the effects of substitution regiochemistry − it is most useful to begin discussing these effects by comparing the systems **1** → **2** and **3** → **4**, where the substituents are shifted to the lateral core positions but are still appended to the same terminal thiophene rings. In general, the mobilities and $I_{on}:I_{off}$ ratios of **2** and **3** are significantly smaller than those of **1** and **2**, respectively, but much larger than

(30) Torsi, L.; Lovinger, A. J.; Crone, B.; Someya, T.; Dodabalapur, A.; Katz, H. E.; Gelparin, A. *J. Phys. Chem. B* **2002**, *106*, 12563.

(31) For **α6T** films, high-temperature annealing was demonstrated to decrease semiconducting performance. Torsi, L.; Dodabalapur, A.; Katz, H. E. *J. Appl. Phys.* **1995**, *78*, 1088.

(32) (a) Carlson, D. P.; Schmiegel, W. *Ullmann's Encyclopedia of Industrial Chemistry*; VCH Verlagsgesellschaft: Weinheim, 1988. (b) Pittman, A. G. In *Fluoropolymers*; Wall, L. A., Ed.; Wiley: New York, 1971. (c) Bunn, C. W.; Howells, E. R. *Nature* **1954**, *174*, 549.

(33) Horowitz, G. *Adv. Mater.* **1998**, *10*, 923.

(34) Horowitz, G.; Hajlaoui, R.; Bouchriha, H.; Bourguiga, R.; Hajalaoui, M. *Adv. Mater.* **1998**, *10*, 923.

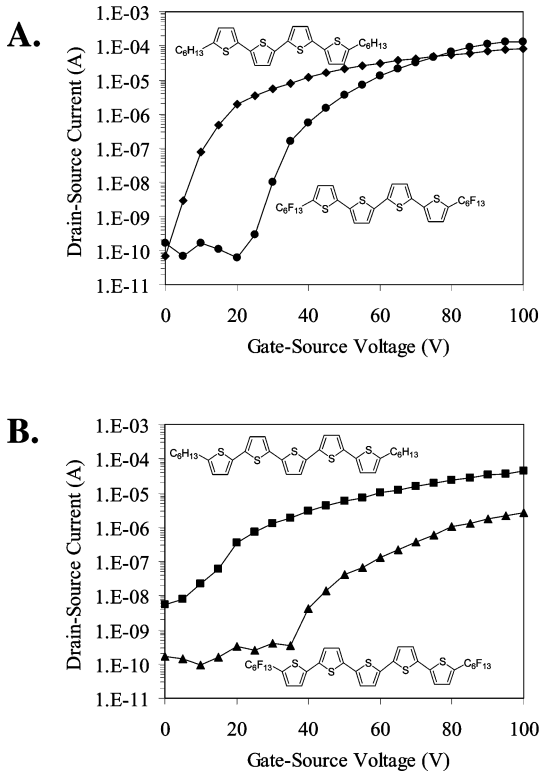

Figure 11. Transfer plots of: (A) **DFH-4T** (●) and **DH-4T** (◆); (B) **DFH-5T** (▲) and **DH-5T** (●).

expected from previous results on β,β'-dialkyl-substituted sexithiophenes. In particular, **isoDH-6T** (at $T_D = 70$ °C) exhibits a mobility of 0.064 $cm^2/(V\ s)$, identical to that of **DH-6T** and with an even larger $I_{on}:I_{off}$ ratio, probably due to the increased band-gap[13] and consequent reduction of the off current. Therefore, lateral substitution decreases intermolecular interactions (evidenced by decreased melting point, increased solubility) but does not sufficiently inhibit solid-state core packing to compromise high mobility. In addition, the difference in mobilities between **1** ↔ **2** and **3** ↔ **4** increases with the compression of the core dimensions ($n = 6 \rightarrow 4$). Because all of the films deposited at 70 °C are highly crystalline, the specific morphologies of **isoDFH-5T** and **isoDH-5T** (circular, isolated grains) versus the smoother **isoDFH-6T** and especially **isoDH-6T** are likely to play a role. However, while **isoDFH-4T** films are highly textured and smooth, the FET response is significantly reduced versus both **isoDFH-6T** and **DFH-4T**. Considering these data in view of the observed lower mobility of **isoDFH-5T** versus **isoDH-5T** (despite similar microstructures and morphologies), it appears that the decreased core conjugation, due to the larger inter-ring torsion in the isoDFH-nT family[13] is also an important element affecting FET performance.

The present results are additionally informative when **iso2DFH-6T** (**6**) and **iso3DFH-6T** (**7**) are considered. In contrast to both **DFH-6T** and **isoDFH-6T**, the fluorocarbon substituents are located in the middle or the very central thiophene rings of the 6T core. The films of these compounds grown both at 25 and 70 °C are quite rough and the XRD spectra of 50 nm thick films exhibit at most very weak reflections, indicating largely amorphous solid-state structures. This is additional evidence (also seen by optical spectroscopy) that the packing characteristics of **6** and **7** are very different from those of **1**−**5**. Not surprisingly, the FET performance (Figure S8) of these films is extremely poor, but measurable, with mobilities in the range $\sim 10^{-6}-10^{-8}$ and $I_{on}:I_{off}$ ratios of 5−10. Interestingly, these systems are p-type semiconductors, and, when a positive bias is applied to the gate, no modulation of the drain−source current is observed. These systems are the second example, in addition to perfluoroarene-thiophene oligomers,[8a] of regiochemically induced modulation of majority carrier sign.

A critical question next arises as to the origin of the "switch" in carrier mobility, from p- to n-type, ongoing from alkyl- and unsubstituted oligothiophene **3**−**5** to the fluorocarbon-substituted systems **1** and **2**, and why **6** and **7** do not adhere to this trend. Among the conceivable factors governing FET behavior[6e,8,35] are the molecular HOMO/LUMO energy positions, the relative electron/hole bandwidths, the nature of the polaronic structures, impurity concentrations, and the screening by the fluorocarbon chains of O_2-promoted inhibition of electron transport. In the present case, the latter two factors are arguably less important because **1**−**7** have been extensively purified (if undetectable quantities of impurities are present, they should have comparable effects for all fluorocarbon-functionalized systems, because similar synthetic pathways and intermediates are employed in the syntheses) and reproducible measurements were carried out for **6** and **7** under high vacuum ($\sim 10^{-6}$ Torr). In most measurements, decreasing the measurement chamber pressure and/or increasing the pumping time increases the mobility of both p- and n-type materials, hence **6** and **7** become better p-type conductors under vacuum. Therefore, the effect of reversible O_2 absorption appears to diminish mobility but is not a factor affecting the intrinsic majority carrier sign. Differences in polaronic structure (preferential localization of charge on the terminal thiophene rings) should already be reflected in the electrochemical redox potentials. Therefore, we suggest that the principal factors governing FET activity characteristics are related to the intrinsic positions of the molecular/solid-state orbitals/bands with respect to charge injection and transport. The strong electron-withdrawing characteristics of the perfluoroalkyl substituents, which affect the frontier orbital energies, must play a decisive role in the carrier sign inversion mechanism. It will be seen below that the electron-withdrawing strength of the perfluoroalkyl substituents is sufficient to lower both the fluorinated-nT HOMO and the LUMO energies such that electron injection and transport becomes, in the majority of cases, more favorable than hole injection and transport. Although these energetic changes are relatively small (0.2−0.6 eV as quantified by the electrochemically derived HOMO/LUMO energies),[13] we show in the next section that small variations in HOMO/LUMO energies can lead to dramatic variations in relative hole and electron injection rates. This prediction may not be appropriate in the case of **6** and **7** for the following reasons: (i) These systems have considerably different solid-state/film structures than **1**−**5**, and consequently the energetic trends found experimentally (in dilute solution) and theoretically (gas phase) may not be equally applicable to the solid-state structures. (ii) The nanostructural and electronic nature of the electrode/semiconductor interface may not be identical.

(35) Cornil, J.; Beljonne, D.; Calbert, J.-P.; Bredas, J.-L. *Adv. Mater.* **2001**, *13*, 1053.

Table 3. Summary of Representative Computed Electronic Structures, Relative to **DFHCH$_2$-6T** with HOMO and LUMO Energies in eV, and Relative Hole (R^{h+}) and Electron (R^{e-}) Injection Rates and Charge Injection Rate Ratio Given in Orders of Magnitude Difference

compound	relative HOMO energy (eV)	relative LUMO energy (eV)	ln(R^{h+})	ln(R^{e-})	ln R^{h+}/R^{e-}
DFHCH2-6T	0.000	0.000	0.00	0.00	0.00
DFH-2T	−1.469	0.027	−56.83	−1.05	−55.78
DFH-3T	−0.925	−0.109	−35.78	4.21	−39.99
DFH-4T	−0.626	−0.109	−24.21	4.21	−28.42
DFH-5T	−0.408	−0.218	−15.79	8.42	−24.21
DFH-6T	−0.245	−0.272	−9.47	10.52	−20.00
isoDFH-2T	−1.633	0.490	−63.15	−18.94	−44.20
isoDFH-3T	−0.925	0.136	−35.78	−5.26	−30.52
isoDFH-4T	−0.626	0.136	−24.21	−5.26	−18.94
isoDFH-5T	−0.381	0.000	−14.73	0.00	−14.73
isoDFH-6T	−0.218	0.000	−8.42	0.00	−8.42
iso2DFH-6T	−0.435	0.027	−16.84	−1.05	−15.79
iso3DFH-6T	−0.435	−0.082	−16.84	3.16	−20.00
DH-2T	−0.190	1.279	−7.37	−49.46	42.10
DH-3T	0.082	0.762	3.16	−29.47	32.63
DH-4T	0.190	0.490	7.37	−18.94	26.31
DH-5T	0.245	0.327	9.47	−12.63	22.10
DH-6T	0.272	0.218	10.52	−8.42	18.94
isoDH-2T	−0.218	1.333	−8.42	−51.57	43.15
isoDH-3T	0.054	0.816	2.10	−31.57	33.68
isoDH-4T	0.054	0.599	2.10	−23.15	25.26
isoDH-5T	0.136	0.408	5.26	−15.79	21.05
isoDH-6T	0.299	0.218	11.58	−8.42	20.00
2T	−0.517	1.034	−20.00	−39.99	20.00
3T	−0.190	0.599	−7.37	−23.15	15.79
4T	0.000	0.354	0.00	−13.68	13.68
5T	0.082	0.190	3.16	−7.37	10.52
6T	0.163	0.109	6.31	−4.21	10.52
C60	−1.034	−0.925	−39.99	35.78	−75.78
NTCDA	−2.748	−1.714	−106.30	66.30	−172.60

DFT Computations. Modeling the Charge Injection Process. Very recently,[13] we showed that DFT calculations reproduce various nT experimental crystal structure molecular geometries well and computed HOMO and LUMO energetic trends[36] are in good accord with experimental electrochemical data. Substitution of oligothiophenes with *n*-hexyl groups at the end-termini (DH/isoDH-nTs) raises both HOMO and LUMO energies versus the unsubstituted oligothiophenes (αnT), while *n*-perfluorohexyl groups (DFH/isoDFH-nTs) lower both groups of energy levels. For example, we find energy differences of +0.11 eV for the **DH-6T** HOMO and LUMO versus **α6T**, and −0.41 and −0.38 eV for the **DFH-6T** HOMO and LUMO, respectively, versus **α6T**. These changes in electronic structure and energies are modest compared to the computed differences between **α6T** and known n-type conductors such as C_{60} and NTCDA (−1.03 and −2.26 eV for the LUMO levels of C_{60} and NTCDA, respectively, vs α6T). Table 3 reports the computed HOMO/LUMO energies relative to **DFHCH$_2$-6T**. Below, we propose a model for how the relative rates of hole and electron injection into these materials depend on oligothiophene orbital energetics.

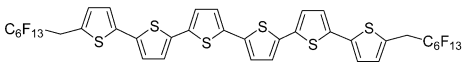

DFHCH$_2$-6T

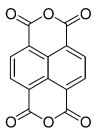

NTCDA

The simplest picture for a Schottky-type injection barrier for hopping-type carrier transport can be described by a Boltzmann-like distribution[37] (Figure 12A) and can be expressed as:

$$\text{rate} \propto e^{-\Delta E/k_b T} \qquad (2)$$

where ΔE is the magnitude of the injection barrier, $T = 298$ K, and k_b is the Boltzmann constant. Although eq 2 is an oversimplified picture of charge injection because it does not explicitly incorporate space charge, image, or interfacial dipole layer effects, and holds approximately only for $\Delta E > 0$, experimental data show it to satisfactorily describe the properties of metal/organic interfaces, in OFETs or OLEDs,[37] and it is physically reasonable to assume that the effects enumerated above remain essentially constant across a related series of compounds. This is especially reasonable for the case of oligothiophenes **1**−**5** considering the striking similarities in their packing motifs and film microstructures. With this exponential dependence of carrier injection rate on ΔE, differences of a few tenths of an eV in the barrier height can significantly affect the injection characteristics. For OFETs, neutral (undoped) compounds are used as the active materials, because low carrier concentrations ensure low current in the "off" state. Therefore, within the assumptions stated above, the relative carrier injection barriers should be describable as the difference between the molecular HOMO energy and the metal electrode work function for hole injection, and the difference between the molecular LUMO energy and the metal electrode work function for

(36) We use HOMO and LUMO as convenient shorthands, because electronic states, not levels, are actually measured.
(37) (a) Mahapatro, A. K.; Ghosh, S. *Appl. Phys. Lett.* **2002**, *80*, 4840. (b) Chwang, A. B.; Frisbie, C. D. *J. Phys. Chem. B* **2000**, *104*, 12202.

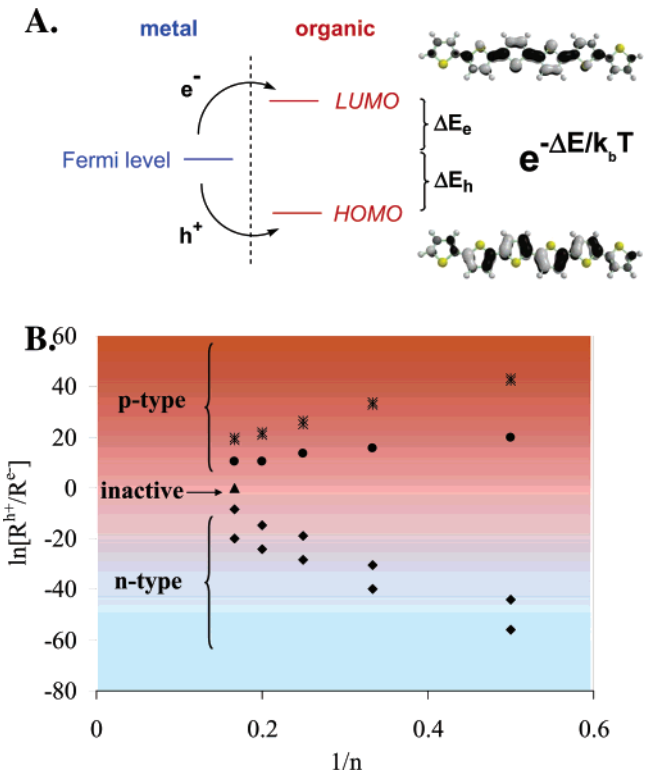

Figure 12. (A) Schematic of a Schottky-type barrier between a metal and an organic semiconductor, showing electron and hole injection barriers and the HOMO and LUMO orbital contours for oligothiophenes. Core substituents do not significantly change the spatial distributions of these orbitals. (B) Plot of computed charge injection rate ratio for oligothiophenes **1**−**5** [DFH-/isoDFH-nTs (◆); αnTs (●); DH-/isoDH-nTs (∗) relative to unsubstituted **DFHCH$_2$-6T** (▲) versus 1/*n* (*n* = oligothiophene core length). The color region denotes the experimental results.

electron injection. Using this definition, we have computed hole and electron injection rates for a broad series of conductors relative to the HOMO and LUMO levels of **DFHCH$_2$-6T**, and the results are summarized in Table 3. **DFHCH$_2$-6T** was arbitrarily chosen as the reference because the molecular components and molecular arrangement on the substrate surface of the vacuum-deposited films are similar to those in systems/films **1**−**5**, and **DFHCH$_2$-6T** is found to be FET inactive, thus neither n-type nor p-type.[38]

From the relative HOMO and LUMO energies of **1**−**5**, C_{60}, and NTCDA, clear trends in charge injection rates relative to **DFHCH$_2$-6T** are apparent. First, we consider the longest 6T systems because both experimentally and theoretically their frontier levels are the closest in energy (due to dilution of substituent effects) to **DFHCH$_2$-6T** and consequently they should lie closer to the borderline separating p- and n-type behavior. As compared to **DFHCH$_2$-6T**, the **α6T** and **DH-6T** barriers to hole injection are decreased by 0.16 and 0.27 eV, respectively, which corresponds to a predicted increase in hole injection rates of $\sim 10^2$ and 10^5, respectively. Similarly, the barrier to electron injection in **DFH-6T** is decreased by 0.27 eV, corresponding to a decrease in injection rate of $\sim 10^5$. These results are in agreement with the experimental majority charge carrier signs observed here in these materials (Table 2). In regard to the shorter oligomers, the barrier for hole/electron injection increases (as compared to **DFHCH$_2$-6T**) when $n = 6 \rightarrow 2$, and for very short oligomers of series **1**, **2** and **3**−**5**, the respective computed electron and hole injection barriers are even larger than in **DFHCH$_2$-6T**. Note that when the electron injection barriers for **1**, **2** and the hole injection barriers for **3**−**5** are compared to the corresponding complementary charge (hole and electron, respectively) injection barriers (Table 3), the decrease in electron injection rate in **1**, **2** and hole injection rate in **3**−**5** in response to contracted core dimension ($n = 6 \rightarrow 2$) is accompanied by an even larger decrease in complementary charge (hole/electron) injection rate. Therefore, the balance between these two parameters can drive the system further toward exclusive n- or p-type activity. In the present picture, the ratio between complementary charge injection rates (Table 3 compiles the hole/electron ratios) should provide a quantitative prediction of the probability that the material is predominantly hole (or electron) transporting relative to inactive **DFHCH$_2$-6T** and a measure of the "competition" between hole and electron majority carrier behavior. This parameter also takes into account the fact that in these semiconductors there is likely a contribution to the observed current from both hole and electrons; hence predominant but not necessarily exclusive conduction is provided by one carrier.

This situation is represented in Figure 12B, where the hole/electron injection ratio is plotted versus the reciprocal of the core dimension (1/*n*). In this plot, charge injection ratios for fluoroalkyl- and alkyl-/unsubstituted families clearly fall into distinct regions with inactive **DFHCH$_2$-6T** acting as a divider between predicted n- (bottom) and p-type (top) regions. Importantly, the present model is in complete agreement with the experimental majority carrier sign results for series **1**−**5** (Table 2). Furthermore, it suggests that from an energetic viewpoint, oligothiophenes with longer cores are more "labile" in terms of their carrier sign; hence a switch between p- and n-type activity is more likely in 6T-type materials than in the corresponding 2T derivatives. For outlyers **iso2DFH-6T** and **iso3DFH-6T**, this picture computes hole/electron injection ratios of $e^{-6.86}$ and $e^{-8.68}$, respectively, which are between those of **DFH-6T** ($e^{-8.68}$) and **isoDFH-6T** ($e^{-3.66}$), and, consequently, predicts n-type activity. The experimental p-type behavior can be partially explained by considering the large difference in solid-state packing characteristics of these systems versus the other oligothiophenes, which likely alters details of the semiconductor−metal interface. Particularly, regiochemical modifications displacing the perfluorohexyl substituents from the molecular periphery may, in turn, orient these substituents away from the metal/organic interface and increase the electron-injection barrier due to increased interface dipole effects.[37−39]

As noted above, the present oversimplified Schottky barrier model does not explicitly treat differential electrostatic and covalent effects on the charge injection barrier which could, in principle, be significant.[37,39] Thus, an intrinsic electron injection barrier of ∼2.8 eV is estimated for a DFH-nT−Au interface (assuming a 5.4 eV Au work function)[40] in the absence of level shifting and image effects. However, as noted above, such effects are reasonably assumed to be constant over a closely related series of molecules, and indeed this is supported by experimental UPS data, evidencing a uniform vacuum level shift

(38) Hong, X. M.; Katz, H. E.; Lovinger, A. J.; Wang, B.-C.; Raghavachari, K. *Chem. Mater.* **2001**, *13*, 4686.
(39) Ishii, H.; Sugiyama, K.; Ito, E.; Seki, K. *Adv. Mater.* **1999**, *11*, 605.
(40) *Handbook of Chemistry and Physics*; CRC Press: Boca Raton, FL, 1995.

across metal−oligothiophene interfaces.[41] In summary, the present results demonstrate that a simple Schottky barrier picture provides excellent predictive guidance as to the majority carrier type for a widely studied class of organic conductors, arguing also that the majority carrier sign measured in OFETs of such materials is largely governed by injection characteristics. Future refinements will focus on including in this model the analysis/prediction of absolute metal−organic interfacial barrier heights and interfacial dipole layer[42] effects.

Conclusions

The thin film properties of a broad series of oligothiophene families **1**−**7** incrementally differing in core size, substitution positions, nature of substituents, and semiconducting behavior have been studied under identical experimental/theoretical conditions. Relevant molecular/solid-state properties of **1**−**5** have been described recently,[13] which provides the basis for predicting/understanding film properties/response. The new 6T derivatives **iso2DFH-6T** (**6**) and **iso3DFH-6T** (**7**) have been designed to address specifically the effects of fluorocarbon-chain regiochemistry on the FET response.

XRD $\theta-2\theta$ investigation indicates that, for room-temperature growth, films of fluorocarbon-substituted **1** and **2** are less crystalline than the corresponding **3**−**5** systems. However, small increases in deposition temperatures or short annealing of room-temperature deposited films affords highly textured materials. For 60−80 °C film deposition temperatures, all of the systems are highly crystalline, and plotting of the observed *d* spacings versus core length (*n*) affords linear correlations. This is evidence that within each film series, the alignment of the molecules and, more importantly, of the molecular components (cores and chains) is essentially independent of core length. Furthermore, similarities between *d* spacings, computed/experimental molecular lengths, and derived core/chain tilt orientations between **1**/**2** and **3**/**4**, respectively, are evidence that fluorocarbon- and alkyl-substituted oligothiophenes have almost identical microstructures. A film morphology study by SEM reveals that film crystallite dimensions generally increase as growth temperature increases. However, the SEM micrographs also reveal that the film grain dimensions for **1** and **2** deposited at room temperature are smaller and much less interconnected than those for the films of the other series. Again, the effect of the temperature is much more evident in the fluorinated films, with crystal dimensions increasing dramatically at higher film growth temperatures or by annealing.

TFT devices were fabricated and characterized using identical $Si-SiO_2$ substrates, device geometries and configurations, as well as instrumentation/environment. Our results clearly demonstrate the crucial importance of oligothiophene core substitution in determining the p- or n-type activity of the semiconductor. Fluorocarbon systems **1** and **2** are majority carrier electron-transporting materials, while fluorine-free systems **3**−**5** are majority carrier hole-transporting semiconductors. Because **1**−**5** have identical core structures, and because the molecular alignment in the corresponding films is either identical or comparable, it is likely that charge injection (barrier height at the electrode−organic interface) and transport (charge hopping between molecules) in the device channel occur in a similar manner among these systems. Therefore, the switch-over from p- to n-type majority carrier activity must be identified primarily with the electron-withdrawing capacities of the fluorocarbon substituents, yielding changes in the relative nT HOMO and LUMO energy positions. Trends in charge carrier mobilities and I_{on}:I_{off} ratios between and within these series are readily understandable considering the interplay of molecular structure and film microstructure and morphology. The films that exhibit the greatest carrier mobilities possess the appropriate combination of large grain size and smooth, interconnected morphology, exhibit molecular orientation directed along the substrate normal, and have sufficient core conjugation/length. Two materials, one p- and one n-type, are of particular importance. The first, **isoDH-6T**, is a regiochemically pure, processable semiconductor with high mobility and I_{on}:I_{off} ratio. This system demonstrates that lateral substitution of thiophene oligomers does not necessarily inhibit TFT performance, as is in the case for regioregular polymers.[11] The second distinctive material is **DFH-4T**, which exhibits one of the highest n-type carrier mobility values (0.22 $cm^2/(V\ s)$) and I_{on}:I_{off} ratio so far reported for an n-type transporting material. This system is also soluble and processable, and, in preliminary experiments, cast films from toluene exhibit a mobility of $\sim 10^{-3}$ $cm^2/(V\ s)$.

Finally, we show that a simple Schottky-type injection barrier picture, based on the relative HOMO and LUMO energetics, offers great utility in understanding the origin of the majority carrier sign. The model yields the relative injection rates of electrons and holes into the organic solid from a metal electrode. The model achieves excellent agreement between theory and experiment, even reproducing subtle features such as inversions in carrier sign in response to changes in oligothiophene substitution pattern and materials which are inactive in thin film transistor configurations. One interesting implication of these results is that the measured carrier sign appears to be largely dominated in these materials by carrier injection characteristics rather than by bulk transport properties. Further studies will focus on the implications of these results.

Acknowledgment. We thank ONR (N00014-02-1-0909) and the NSF-MRSEC program through the Northwestern Materials Research Center (DMR-0076097) for support of this research. This work was also supported by the NASA Institute for Nanoelectronics and Computing under Award Number NCC 2-3163. We thank Dr. Howard Katz for useful suggestions on FET measurements.

Supporting Information Available: Experimental details. Table of selected reflections for a simulated powder pattern of **DFH-3T**, **DFH-4T**, and **isoDFH-5T**. UV−vis spectra of **iso2DFH-6T** and **iso3-DFH-6T**. XRD $\theta-2\theta$ scan of **DFH-2T** (before and after annealing), **DFH-3T**, **isoDFH-5T**, and **isoDFH-6T** films. SEM of **DFH-4T**, **DFH-5T**, **DFH-6T**, and **isoDFH-4T** films. Drain−source current−voltage plots of **iso2DFH-6T** and **iso3-DFH-6T**. This material is available free of charge via the Internet at http://pubs.acs.org.

JA0489846

(41) (a) Fujimoto, H.; Nagashima, U.; Inokuchi, H.; Seki, K.; Cao, Y.; Nakahara, H.; Nakayama, J.; Hoshino, M.; Fukuda, K. *J. Chem. Phys.* **1990**, *92*, 4077. (b) Makinen, A. J.; Hill, I. G.; Kinoshita, M.; Noda, T.; Shirota, Y.; Kafafi, Z. H. *J. Appl. Phys.* **2002**, *91*, 5456. (c) Makinen, A. J.; Hill, I. G.; Noda, T.; Shirota, Y.; Kafafi, Z. H. *Appl. Phys. Lett.* **2001**, *78*, 670.

(42) Crispin, X.; Geskin, V.; Crispin, A.; Cornil, J.; Lazzaroni, R.; Salaneck, W.; Brédas, J.-L. *J. Am. Chem. Soc.* **2002**, *124*, 8131.